A specific gene expression program underlies antigen archiving by lymphatic endothelial cells in mammalian lymph nodes

Ryan M. Sheridan[1], Thu A. Doan [2,3], Cormac J. Lucas [3], Tadg S. Forward [2,3], Ira Fleming [1,2,3], Valerie M. Olsen [2,3], Abrianna M. Qvale[2,3], Bennett J. Davenport [3], Kristen Zarrella [3], Michael G. Harbell[3], Aspen Uecker-Martin[1], Thomas E. Morrison [3], Jay R. Hesselberth [1] & Beth A. Jirón Tamburini [2,3] ✉

Lymph node (LN) lymphatic endothelial cells (LEC) actively acquire and archive foreign antigens. Here, we address questions of how LECs achieve durable antigen archiving and whether LECs with high levels of antigen express unique transcriptional programs. We use single cell sequencing in dissociated LN tissue and spatial transcriptomics to quantify antigen levels in LEC subsets and dendritic cell populations at multiple time points after immunization and determine that ceiling and floor LECs archive antigen for the longest duration. We identify, using spatial transcriptomics, antigen positive LEC-dendritic cell interactions. Using a prime-boost strategy we find increased antigen levels within LECs after a second immunization demonstrating that LEC antigen acquisition and archiving capacity can be improved over multiple exposures. Using machine learning we define a unique transcriptional program within archiving LECs that predicts LEC archiving capacity in independent mouse and human data sets. We test this modeling, showing we can predict lower levels of LEC antigen archiving in chikungunya virus-infected mice and demonstrate in vivo the accuracy of our prediction. Collectively, our findings establish unique properties of LECs and a defining transcriptional program for antigen archiving that can predict antigen archiving capacity in different disease states and organisms.

Viral antigens persist within lymph nodes following viral infection[1–5]. Persisting antigen, in the case of influenza virus infection, can recruit memory T cells, promoting protection against future infections with the same virus[1–3,5–7], demonstrating that persisting viral antigens may be an important mediator of immune memory responses. We demonstrated that protein subunit immunization, administered with a Toll-like receptor (TLR) agonist subcutaneously, also initiates persistence of the protein antigen in the draining lymph node (dLN)[8–11].

Similar to virus-derived persisting antigen, the vaccine-derived persisting antigen improved T cell memory[8,10]. We termed this process of durable antigen retention "antigen archiving"[10].

Lymphatic endothelial cells (LEC)s interact with antigens and virus as they traffic through lymphatic capillaries to lymphatic collectors before entering the lymph node sinus and the fibroblastic reticular cell (FRC) conduit system. These two cell types, LEC and FRC, along with blood endothelial cells (BEC), comprise a larger non-hematopoietic

[1]Department of Biochemistry and Molecular Genetics, RNA Bioscience Initiative, University of Colorado School of Medicine, Aurora, CO, USA. [2]Department of Medicine, Division of Gastroenterology and Hepatology, University of Colorado School of Medicine, Aurora, CO, USA. [3]Department of Immunology and Microbiology, University of Colorado School of Medicine, Aurora, CO, USA. ✉e-mail: Beth.tamburini@cuanschutz.edu

subset of cells within the LN called lymph node stromal cells (LNSC). In recent years many LNSC subtypes have been defined using single-cell RNA-sequencing (scRNA-seq)[11–14], propelling our understanding of the diversity of LNSCs and their contributions to LN function. Despite these advances, the functional roles of LNSC subpopulations are poorly defined. To begin to understand how these different LNSC subpopulations handle antigens, we previously quantified antigen levels across different LNSC subsets and myeloid cell populations using a protein antigen conjugated to a stabilized DNA tag suitable for detection by single cell sequencing[11].

While LECs can present peripheral tissue antigens to promote peripheral tolerance, archived antigens are exchanged to migratory conventional dendritic cells (cDC1 and 2) to promote immunity. Consistent with live imaging and antigen presentation assays, antigen-DNA conjugates were predominantly found in CCR7hi migratory cDCs[11]. Thus, as migratory DCs traffic from the skin to the dLN, they interact with antigen bearing LECs, acquiring antigens to improve the effector function of memory CD8+ T cells[9–11]. Indeed, some antigen is acquired by DCs from LECs that undergo apoptosis during LN contraction[8,9]. We also studied the consequences of immune insult to antigen archiving LECs and found that a subsequent inflammatory stimulus, within the archiving timeframe, caused LEC death and increased T cell effector responses compared to those that did not have a secondary stimulus. These improved T cell effector responses depended on T cell receptor (TCR) stimulation and were independent of bystander activation[8]. Protection from these boosted memory CD8 + T cells was durable and robust, establishing a model wherein cell-mediated immunity can be manipulated by the presentation of previously archived antigens. Collectively, these studies demonstrate an important role for antigen archiving, in promoting protective T cell immunity at late time points after immunization.

LECs acquire multiple types of protein antigens[8–10] including purified chikungunya (CHIKV) viral E2 glycoprotein, albumin, ovalbumin, SARS-Co-V-2 receptor binding domain (RBD)[8], influenza nucleoprotein (NP), herpes simplex virus glycoprotein B (HSVgB), and vaccinia viral proteins post-infection[10]. In addition to acquisition and retention of foreign protein antigens, LECs may support viral replication, such as Kaposi's sarcoma associated herpes virus[15]. Recently, scRNA-seq of LNSCs during CHIKV infection indicated that subsets of LECs that express the scavenger receptor macrophage receptor with collagenous structure (MARCO) may support CHIKV RNA replication[16], consistent with another study showing MARCO-dependent internalization of CHIKV by LN LECs[17]. CHIKV RNA is also detectable in fibroblasts, which express the CHIKV entry receptor MXRA8[18,19]. Although CHIKV infection causes LN disorganization and impaired CD8$^+$ T cell responses[17,20], exploiting this mechanism of viral targeting could lead to a better understanding of the functions of distinct LNSCs. Confirmation of these entry mechanisms used scRNA-seq to detect very low levels of CHIKV RNA within MARCO-expressing LECs[16,17].

In our previous studies of antigen-DNA conjugates, antigen levels were assessed 2 days and 2 weeks post-immunization[11]. More recently[8], we found that the protective capacity of archived antigens was maintained at longer time points (> 2 weeks post-immunization), especially when there was a secondary inflammatory stimulus that caused the release of archived antigens to stimulate memory T cells. However, there are still unanswered questions about how LNSCs archive antigens, including factors that contribute to the duration and maintenance of archived antigens within LECs, whether LECs acquire and retain multiple antigens following sequential immunizations, whether LNSC are intrinsically programmed to archive antigens, whether they learn to archive additional antigens after acquisition, the impact of infection prior to antigen archiving, and if human LNs are also able to participate in LEC antigen archiving.

In this work we detect antigen archiving via a protein conjugated to a DNA tag for use with scRNA-seq and spatial transcriptomics. We find antigen is archived predominantly by subcapsular sinus LECs for 42 days. We demonstrate how antigen high LEC transcriptional programs can predict antigen archiving ability and identify genes important for antigen acquisition and archiving. Furthermore, we show that one immunization leads to an improved ability to archive antigens during a second immunization and that spatially antigen bearing LECs and DCs are in close proximity. Herein, using our predictive models on existing data of CHIKV infected lymph nodes we predict that antigen archiving is impeded and then experimentally test the validity of this prediction. Finally, we outline the importance of antigen archiving in human lymph nodes and demonstrate the utility of the identified gene programs for assessing antigen archiving in other datasets.

Results
Antigen persists in distinct cell populations within the lymph node

To study the dissemination of antigens in the draining lymph node after immunization, we previously developed a scRNA-seq approach to quantify antigen levels in vivo[10] involving conjugation of a model antigen, ovalbumin (OVA), to a DNA barcode containing phosphorothioate linkages (psDNA). Using this tool, we showed that immunization with OVA-psDNA and vaccinia virus (VV) induces robust antigen archiving[9,11]. We identified populations of LNSCs that retain antigen for 14 days post-vaccination and gene expression patterns associated with antigen archiving[11]. The ability of an LEC to archive antigen could be influenced by two separate processes: 1) antigen uptake, which likely occurs through endocytic pathways, and 2) antigen retention, which would be influenced by the cellular compartment where the archived antigen is stored. However, our previous studies[11], lacked the temporal resolution to differentiate between these two processes. Here we sought to evaluate the dynamics of antigen uptake and archiving by performing an extended 42 day post-immunization time-course.

We immunized mice subcutaneously with OVA-psDNA + VV to both track exogenous antigen and induce robust LN expansion and antigen archiving[8,11] and performed scRNA-seq on CD45- cell populations from the dLN at 2, 14, 21 and 42 days post-immunization. In a separate cohort of mice immunized at the same time, we sorted dLN cells into four populations, which were enriched for CD11c + , CD11c-CD11b + , B220+ and all other cells. We performed scRNA-seq using these sorted populations mixed at a ratio of 4:4:1:1 (Figure S1A), respectively[11], in order to acquire adequate numbers of DCs, but still have representation of other cell types in the LN to use as controls. We then compared antigen levels across a time-course using our published scRNA-seq data collected 2 and 14 days post-immunization[11] and new data from 21 and 42 days post immunization (Fig. 1A). To accurately compare cell populations across the four time points, we integrated the scRNA-seq data for each time point and re-annotated the cell types present in each sample using a previously published automated approach[21] (Figure S2A–E). To compare levels of antigen across our datasets we calculated background-corrected antigen scores (Agscore) for each cell, normalizing counts by the total antigen counts for the sample. In support of our previous work, we detected the highest antigen levels within lymphatic endothelial cells (LECs), which correlated with the amount of fluorescent antigen, administered with polyI:C and anti-CD40, over time as evaluated by flow cytometry using MFI (Figure S3A). Antigen amounts were detected in lower levels in neutrophils, blood endothelial cells (BECs), fibroblasts, monocytes, and dendritic cells (DCs) (Fig. 1B, S3B-E). Levels of antigen were highest 2 days post-vaccination (Fig. 1B). In all cell types identified, except LECs, antigen levels dropped sharply by day 14 and were largely undetectable by day 42 (Fig. 1B, S3B–E). LECs maintained high levels of antigen throughout the 21 day time-point, however by day 42 antigen levels were substantially reduced, though still higher than all other cell populations (Fig. 1B). These results support our previous work
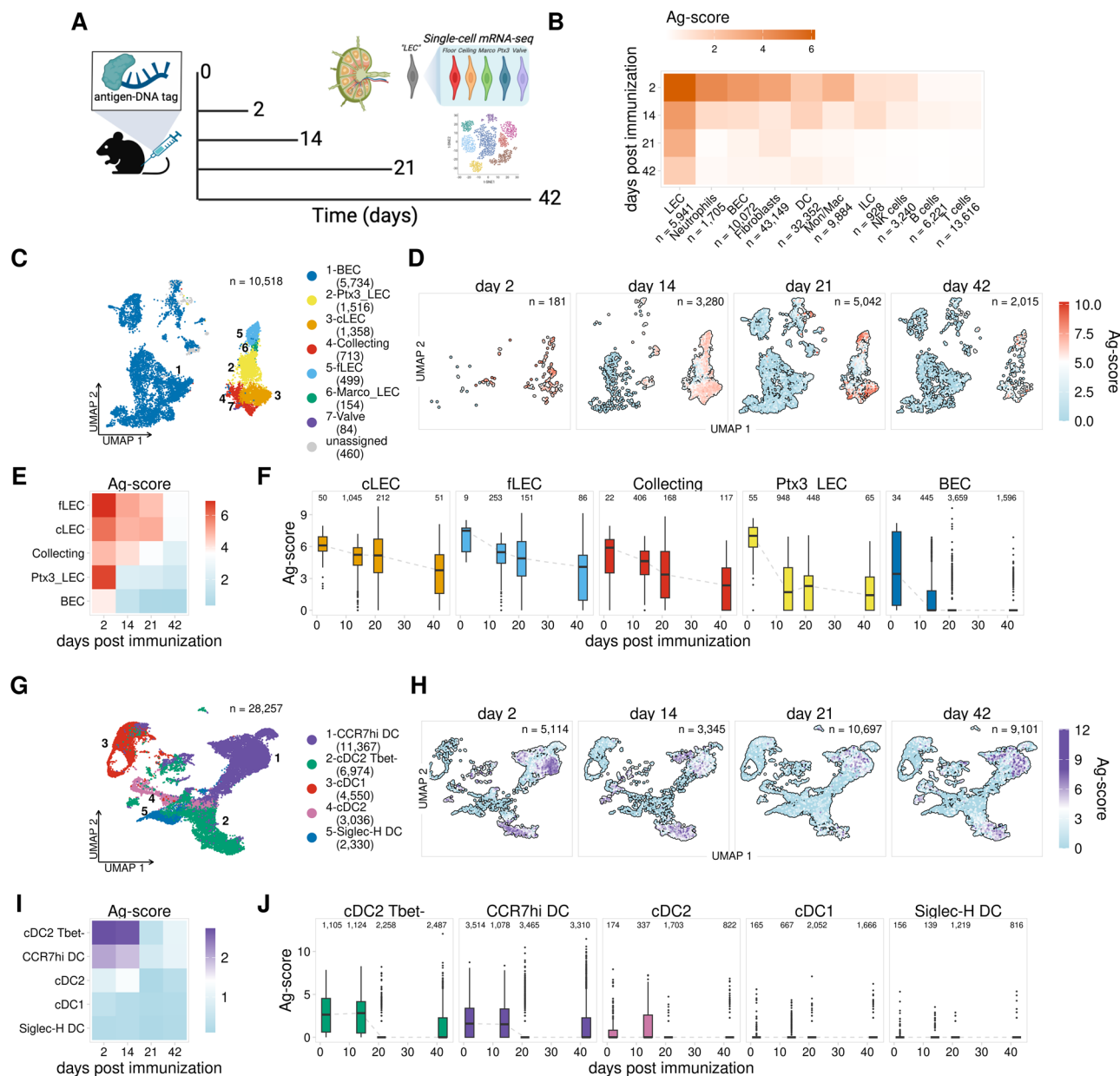
Fig. 1 | Antigen persists in discrete cell populations within the lymph node.
A Experimental design. Created in BioRender. Tamburini, B. (2025) https://BioRender.com/q5mhs3w. **B** Mean Ag-score is shown for each cell type for 2, 14, 21, and 42 days post vaccination. For the 21 and 42 day time points one replicate is shown, a second replicate is shown in Figure S3. For each replicate experiment, 13 mice were used per group where popliteal LNs from 9 mice were pooled for CD45- selection and popliteal LNs from 4 mice were pooled for CD45+ cell enrichment of myeloid cell populations prior to sequencing. **C** UMAP projection shows LEC subsets sequenced after CD45- enrichment of 18 popliteal LNs from 9 mice. **D** UMAP projections show Ag-scores for LEC subsets for each timepoint, replicates described as in (**B**). **E** Mean Ag-score is shown for LEC subsets for each timepoint. Replicates as described in (**B**). **F** Ag-scores are shown for each timepoint for each LEC subset. The number of cells plotted is shown above each boxplot. The center line, box limits, whiskers, and points represent the median, interquartile range (IQR), the range within 1.5×IQR from the box limits, and points outside this range (outliers), respectively. One biological replicate is shown as described in (**B**). **G** UMAP projection shows DC subsets from 8 popliteal LNs per group combined and sequenced after sorting shown in Fig. S1A where CD11c + , CD11b + , B220+ and "other" cells were recombined at a 4:4:1:1 ratio post sorting. One replicate is shown. A second replicate is show in Figure S3. **H** UMAP projections show Ag-scores for DC subsets for each timepoint, replicates described as in (**B**, **F**). **I** Mean Ag-score is shown for DC subsets for each timepoint as described in (**E**). **J** Ag-scores are shown for each timepoint for each DC subset as described in (**F**).

showing that LECs are the predominant cell population that acquires and archives antigens in the draining lymph node[11].

To investigate the dynamics of antigen acquisition and archiving across different LEC subsets, we next annotated different endothelial cell populations using previously published data[11,14] (Figure S2B, D). Using this approach, we identified subsets of valve and collecting LECs that form the afferent and efferent collecting vessels of the lymph node (collecting LECs) (Fig. 1C, S2B, D), as well as floor (fLEC) and

ceiling (cLEC) LECs of the subcapsular sinus (SCS), which express the adhesion molecule Madcam1 and the atypical chemokine receptor Ackr4, respectively (Fig. 1C, S2B, D). SCS LECs are the first LEC populations that encounter lymph-borne antigens after entry into the lymph node and we previously showed that these populations have the highest levels of antigen 14 days post-immunization[11]. We also identified LEC subsets from the medullary and paracortical sinuses, which are distinguished by the expression of the scavenger receptors

MARCO (Marco LECs) and Ptx3 (Ptx3 LECs)[11,14,16,17] (Fig. 1C, S2B, D). Analysis of antigen levels over time for each LEC population revealed that at 2 days post-immunization, LECs show universally high levels of tagged antigen (Fig. 1D–F, S3B, D). These findings indicate that immediately following a protein subunit immunization, antigen is dispersed throughout the LN, including in Marco and Ptx3 LECs, which are among the last populations to encounter antigen, based on the spatial locations of these subsets as identified by others[14]. However, antigen levels at later times after immunization showed significant differences in antigen archiving ability. We detected high antigen levels in valve LECs, cLECs, fLECs, collecting LECs, and Marco LECs through 21 days post-immunization, while antigen levels drop significantly by day 14 in Ptx3 LECs (Fig. 1D–F, S3D). These results indicate that differences in antigen archiving are not due to LEC localization within the lymph node or efficiency of antigen uptake, as we observe high amounts of antigen within all LEC populations 2 days after immunization, and instead suggest that the dynamics of antigen archiving are a key determinant of overall antigen levels.

The protective capacity conferred by antigen archiving is dependent on antigen exchange with migratory DCs, which present archived antigen peptides to memory CD8+ T cells[8,9]. To explore the dynamics of antigen exchange between LECs and different DC subsets, we integrated the DC datasets for each time point and annotated specific DC populations using previously published data[11,22,23], identifying conventional (c) DC1 and DC2 populations along with CCR7hi migratory cDCs and Siglec-H-expressing plasmacytoid DCs (Fig. 1G, S3C, E). Comparison of antigen levels between these populations showed cDC2 Tbet- and CCR7hi DCs had the highest antigen levels 2 days post-vaccination, with other subsets having minimal levels at any time point (Fig. 1H–J, S3E). The CCR7hi and Tbet- DC subsets both showed consistent levels of antigen through day 14, with levels dropping sharply by day 21. These findings are consistent with other reports demonstrating the length of time DCs remain viable after activation[24]. Therefore, we suggest that any antigen remaining within the DC populations beyond 2–3 weeks is likely a result of DC acquisition of antigen from other cell types. Consistent with our published data that migratory DCs are required for antigen exchange, it is likely the antigen positive DCs remaining have acquired antigen from the only cell type with appreciable antigen at these late time-points, LECs.

Identification of gene signatures associated with antigen archiving by LECs

Comparison of antigen levels throughout the time course revealed significant differences in antigen archiving between LEC populations. We next identified gene expression signatures that might influence the ability of different LEC subsets to archive antigen. We sought to leverage our new scRNA-seq data to characterize gene expression programs underlying antigen archiving. We first identified LECs with high levels of antigen (Ag-high) at the day 14 time point by performing k-means clustering separately for each LEC subset using the calculated antigen scores (Fig. 2A). To ensure consistent classification of Ag-high cells across the time points, we used the day 14 antigen score cutoffs to classify antigen-high (Ag-high) cells in the day 21 and 42 time points.

To investigate gene expression patterns underlying antigen retention, we next identified the top genes that showed the greatest differences in expression between Ag-high and -low populations. Using these genes, we trained two distinct models for each LEC subset, a gradient boosting machine model (GBM, model 1) and a deep neural network (model 2) (Supplementary data 1). We trained these models using day 14 cLECs, fLECs, and collecting LECs, which showed the highest levels of archived antigen at this time point. Valve and Marco LECs also exhibited higher levels of antigen throughout the time course, however, the relatively small number of cells identified in these subsets precluded them from downstream analysis (Figure S3D). Using

these models, we identified genes most predictive of whether an LEC from one of these subsets would archive high or low amounts of antigen. We then grouped these genes into distinct Ag-high and Ag-low gene programs based on whether the gene showed higher or lower expression in Ag-high cells, respectively (Supplementary data 2). We found that the gene programs identified for each LEC subset are distinct and have relatively few overlapping genes (Figure S4A). To characterize cellular processes potentially influencing antigen archiving, we identified gene ontology terms for the Ag-high and -low gene programs for each LEC subset (Figure S4B, C, Supplementary data 3). From this analysis, we found that the Ag-high programs are enriched for genes suggestive of increased endosomal-lysosomal function (Figure S4B, C, Supplementary data 3), and this is most significant for cLECs and fLECs. This includes endosome and lysosome factors with broad roles in protein homeostasis (Ctsd[25], Grn[26], Lgmn[27], Prcp[28]), endosomal trafficking (Vps13b[29], Vps41[30], Vps52[31]), lipid metabolism (Psap[32]), and lysosome acidification (Atp6ap1[33]). In addition, expression of the clathrin adaptor protein Dab2[34] may indicate increased endocytic activity. Consistent with differences in endocytic activity we previously identified genes associated with caveolin-mediated endocytosis that are expressed more strongly in LECs with higher levels of archived antigen at day 14[11]. The collecting LEC Ag-high module also includes genes related to endosomal-lysosomal function (Atp6v1h[35]), however, this module is more strongly associated with broader endothelial cell activation. This includes genes related to cell migration (Rock2[36]), inflammatory signaling (Nfat5[37]), cell proliferation (Tgfa[38]), and extracellular matrix (ECM) remodeling (Tgm2[39]). Analysis of the Ag-low gene programs show enrichment of genes associated with established structural and functional roles of LECs (Figure S4C, Supplementary data 3). This includes genes that promote lymphangiogenesis (Hmgb1[40]), ECM factors that provide structural support for lymphatic vessels (Col4a2, Lamc1, Lama4, Nid2, Fn1)[41,42], and genes involved in immune cell trafficking (Ccl21a[43]).

To further investigate how these gene programs could impact antigen archiving, we next assessed whether Ag-high genes were induced in response to an immune stimulus. We compared each time point after immunization with previously published scRNA-seq data from sorted LNSCs of naïve mice[17]. We found that these programs are robustly expressed in LECs from naïve mice and expression persists 42 days post-vaccination when most archived antigen has been released or degraded (Figure S4D, E). These findings suggest that naïve LECs that express the gene program are predisposed to archive antigen. Furthermore, the Ag-high gene modules were most highly expressed in the LECs and not other cell types (e.g., BECs and DCs) (Figure S4F–H). These findings suggest that the identified gene programs are expressed by most LECs regardless of whether they were immunized, however, as the module score increases in cLEC, fLEC and collecting LEC populations at some timepoints between d2 and d42 compared to d0 (naïve) (Fig. S4D, E) some genes within the program are likely to be specifically induced in response to the immunization. Together these results support a distinct program where Ag-high LECs, which have a transcriptome shifted towards increased endo-lysosomal activity, are equipped to acquire and process a higher volume of internalized material (e.g. foreign protein antigens). The high levels of antigen acquired by LECs are therefore likely to contribute to the length of antigen duration, consistent with prior work[10].

Continued expression of the Ag-high gene program in cLECs, fLECs, and collecting LECs after 21 and 42 days post immunization (Figure S4D) suggests there are a fraction of LECs that are competent to archive antigen even though most antigen has been degraded or released by these time points. To further investigate these potential archiving-competent cells, we attempted to identify LEC populations that would be predicted to archive antigen at the 21 and 42 day time points, based on the classification models trained using the day 14
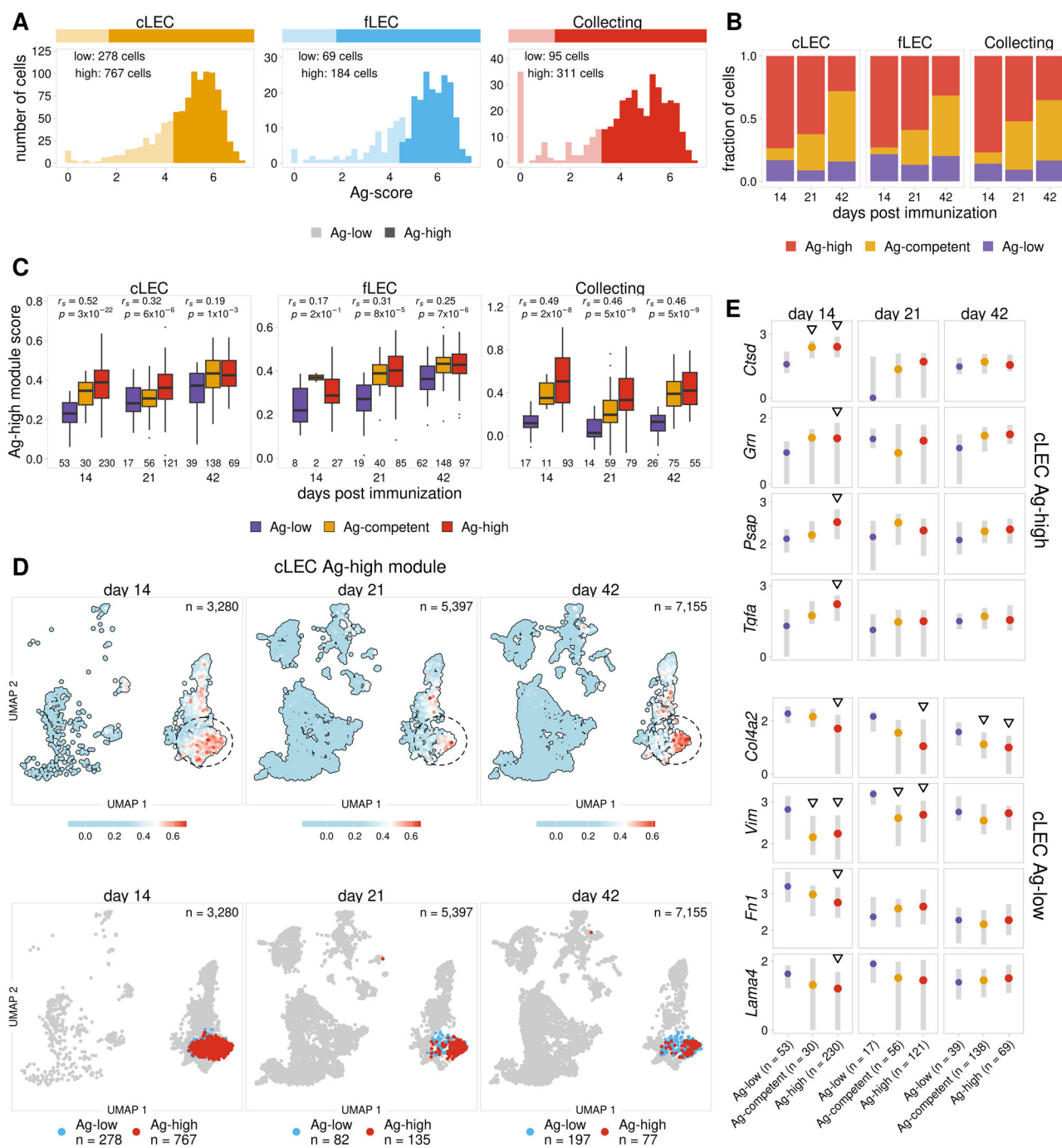
Fig. 2 | Identification of an antigen archiving gene signature. A Ag-score is shown for day 14 Ag-high and -low cells identified for LEC subsets with the highest Ag-scores. **B** The fraction of cells predicted to be Ag-competent is shown for each LEC subset 14, 21, and 42 days post vaccination. Cells shown were not used for training models. **C** Ag-high module score is shown for Ag-low, Ag-high, and predicted Ag-competent LECs. Cells shown were not used for training models. The Spearman correlation between the ordered antigen classes and Ag-high module scores is shown for each timepoint. One-sided *p*-values testing for an increase in module score were calculated and adjusted using Benjamini-Hochberg correction. The center line, box limits, whiskers, and points represent the median, interquartile range (IQR), the range within 1.5×IQR from the box limits, and points outside this range (outliers), respectively. The number of cell plotted is shown below each boxplot. **D** UMAP projections show cLEC Ag-high module scores for each timepoint (top) and Ag-high and Ag-low cLECs (bottom). **E** The expression of select genes from the Ag-high (top four) and Ag-low (bottom four) gene modules is shown for cLECs. Triangles indicate the gene is differentially expressed (*p*-value < 0.05) when compared to Ag-low cells. *P*-values were calculated using a one-sided Wilcoxon rank sum test with Benjamini-Hochberg correction. Points indicate the median and grey bars show the interquartile range.

time point. From this analysis we classified cells into three groups: 1) Ag-low has low amounts of archived antigen based on quantification of antigen scores, 2) Ag-competent has low amounts of antigen but is predicted to have high antigen archiving capability by our classification models, and 3) Ag-high has high levels of antigen. We find that at day 21 and 42 most cLECs, fLECs, and collecting LECs that have low levels of antigen are predicted to be Ag-competent (Fig. 2B, S5A). To assess the accuracy of these predictions, we compared expression of the Ag-high and Ag-low gene modules derived from our day 14 classification models. As expected, we found that the predicted
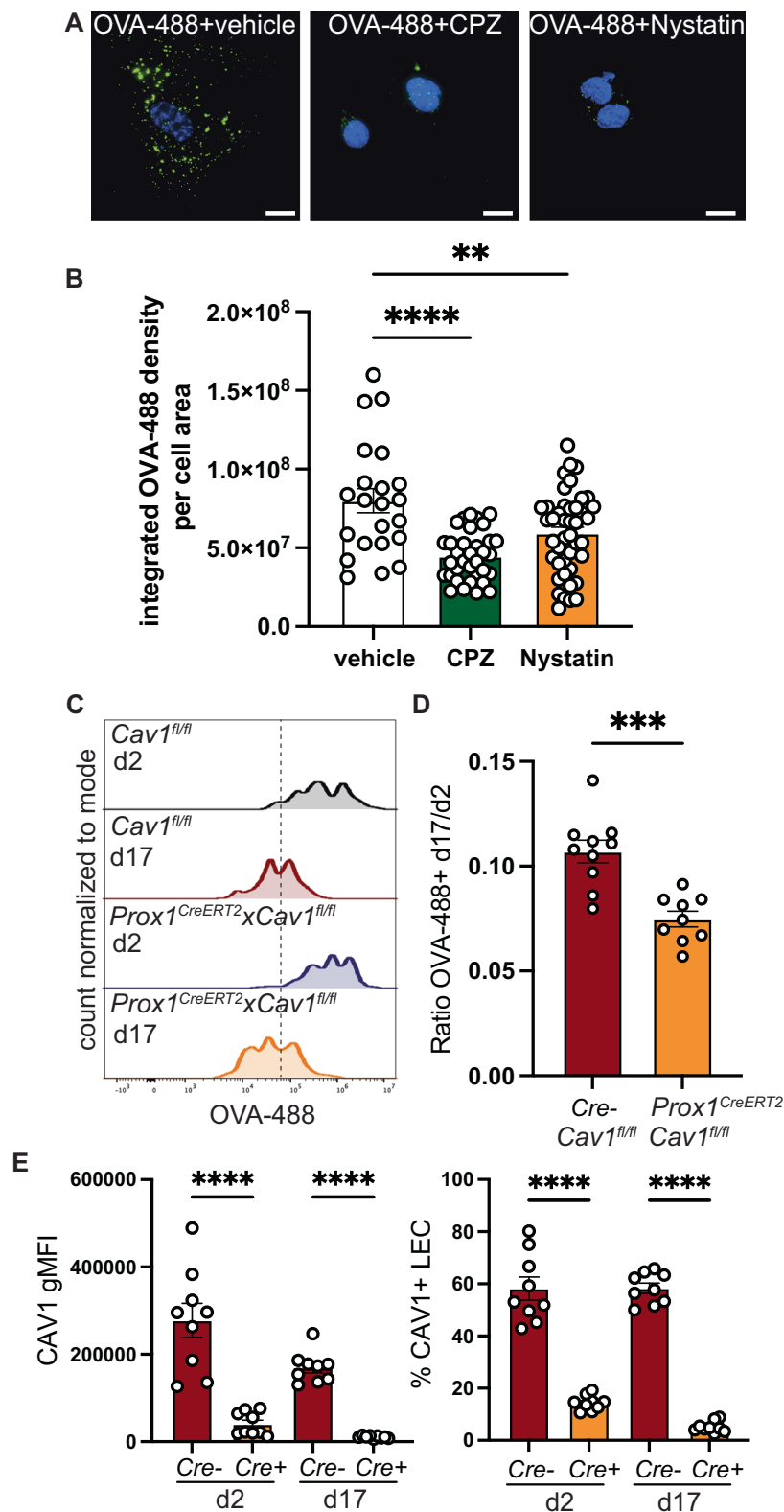
Ag-competent cells have higher expression of the Ag-high module and reduced expression of the Ag-low module when compared with Ag-low cells (Fig. 2C, S5B). Furthermore, by comparing Ag-low, Ag-competent, and Ag-high cells, we found a notable correlation between these classes and the expression of the Ag-high and -low gene programs (Fig. 2C, S5B). We saw that LECs that retain high amounts of antigen at the 21 and 42 day time points generally show the strongest and weakest expression of the Ag-high and -low

programs, respectively (Fig. 2C–E, S5). To summarize, we were able to identify gene signatures (Figure S4A–C, Supplementary data 2) expressed in LECs from naive mice (Figure S4D, E) that are predictive of the capacity of a cell to archive antigen (Fig. 2B, S5A, Supplementary data 1) and correlate with the duration of antigen retention (Fig. 2C, S5B). This information can be used to test whether the Ag-competent cells, that express the Ag-high gene program but are not antigen positive, are more likely to archive a second antigen.

Fig. 3 | Inhibition or deletion of endocytosis pathways limits antigen acquisition and archiving. A Representative images of human lymphatic endothelial cells (LEC)s cultured in chamber slides with vehicle (DMSO), chlorpromazine (CPZ), or nystatin for 1 h prior to culturing with OVA-488 for 2 h. Scale bar =10 μm. **B** Quantification of OVA-488 integrated density per cell area using Image J software. Each dot represents 1 cell. $N = 22$ vehicle treated cells, $n = 33$ CPZ treated cells, and $n = 42$ Nystatin treated cells were evaluated. Experiment was performed on two independent occasions. Data are presented as mean values +/- SEM. Adjusted P-Value **$p = 0.0051$, ****$p < 0.0001$ by one-way ANOVA with two-sided Tukey's multiple comparison test. All data points are shown. **C** $Prox1^{CreERT2}$ positive $xCav1^{fl/fl}$ or $Prox1^{CreERT2}$ negative $xCav1^{fl/fl}$ were treated with tamoxifen for 1 week. Two weeks later mice were immunized with 10 μg OVA-488, 5 μg polyI:C, 5 μg αCD40 per footpad. Representative flow histogram of OVA-488 intensity from LECs (CD45-, CD31 + , PDPN +) at indicated time-points (days (d)) after immunization.

D Quantification of ratio of mean fluorescence intensity of d17 ($n = 9$) and d2 ($n = 9$) for indicated genotypes. Each data point is the geometric mean fluorescence intensity (gMFI) value per sample compared to the average MFI value of D2 per genotype. Each dot represents 2 combined dLNs from 1 mouse where $n = 9$/group. Adjusted p-value ***$p = 0.007$ by one-way ANOVA with Tukey's two-sided multiple comparison test. Data are presented as mean values +/- SEM. Experiment was performed on at least two separate occasions. All data points are shown. **E** Expression levels of caveolin 1 protein (CAV1) in LECs by gMFI of CAV1 or percent of CAV1+ LECs at time of euthanasia in indicated groups after tamoxifen treatment described in part (C). Each dot represents 2 combined draining lymph nodes (dLN)s from 1 mouse where $n = 9$/group. Adjusted p-value ****$p < 0.0001$, by one-way ANOVA with Tukey's two-sided multiple comparison test. Data are presented as mean values +/- SEM. Experiment was performed on at least two separate occasions. All data points are shown.

Antigen acquisition and archiving are mediated in part by clathrin and caveolin mediated endocytosis

In our antigen archiving gene expression modules we identified genes such as *Cavin1* (rank 60) and *Dab2* (rank 162) (Supplementary Data S2) that are important mediators of caveolin mediated endocytosis and clathrin mediated endocytosis, respectively. Caveolin mediated endocytosis uses Caveolin1 (CAV1) and Caveolin2 (CAV2) at the plasma membrane which interact with Cavin 1 (CVN1) and Cavin 2 (CVN2) to stabilize caveolae[44]. *Cav1* is highly expressed in endothelial cell populations and not hematopoietic cell populations[23]. *Dab2* is a clathrin adapter protein and loss of *Dab2* impairs clathrin mediated endocytosis[45]. To investigate whether acquisition of antigen (OVA-488) is mediated by either of these two processes we used human LECs. Cells were treated with vehicle, chlorpromazine (CPZ) or nystatin which inhibit either clathrin or caveolin mediated endocytosis, respectively (Fig. 3A). We observed reduced OVA-488 acquisition by human LECs treated with either CPZ or nystatin (Fig. 3A, B). To further evaluate the requirement of caveolin mediated endocytosis for antigen archiving, we used $Prox1^{creERT2}xCav1^{fl/fl}$ mice to deplete CAV1 from LECs, where caveolin mediated endocytosis is impaired in the absence of $Cav1$[46]. To evaluate antigen uptake (d2) and archiving (d17) we immunized tamoxifen treated mice with OVA-488/polyI:C/αCD40, an immunization strategy previously shown to result in antigen archiving[8–10], and 2 or 17 days later evaluated antigen levels in lymph node LECs by flow cytometry (Fig. 3C, S1B). Antigen fluorescence was similar between cre negative and cre positive groups at 2 days (Fig. 3C). At 17 days antigen fluorescence was lower in the LECs of mice in which *Cav1* was deleted (Fig. 3C). When we evaluated the rate of loss by measuring the fraction of antigen at day 17 compared with day 2, we found a significant reduction in the $Prox1^{creERT2}xCav1^{fl/fl}$ mice (Fig. 3D). This reduction was likely a result of *Cav1* deletion in LECs as both CAV1 mean fluorescence intensity and percent positive were significantly reduced in the LECs of cre+ mice (Fig. 3E). Therefore, genes and gene programs identified in our antigen archiving module, like endocytosis, functionally participate in the maintenance of antigen archiving.

## Antigen archiving by LECs is enhanced by sequential immunization

We have previously shown that a subsequent immune challenge results in the presentation of previously archived antigens, which in turn boosts protective immunity[14]. To expand on these results, we next investigated how the dynamics of antigen archiving are impacted by sequential immunizations administered within the archiving time frame. We compared mice from three vaccination groups, A) received one vaccination 21 days prior to harvest, B) received one vaccination 42 days prior to harvest, and C) received both vaccinations, 42 and 21 days prior to harvest (Fig. 4A). For each group we immunized WT mice with OVA-psDNA+VV subcutaneously, harvested dLN, and performed scRNA-seq on LN populations as described above. To separately quantify archived antigen originating from the immunization

21 days prior to euthanasia (purple syringe) and the immunization 42 days prior to euthanasia (red syringe), the psDNA tags for each immunization contained unique barcodes (barcode (BC)#1 and #2) (Fig. 4A).

To first investigate how previously archived antigen affects archiving during a second immune challenge, we compared levels of the BC#2 antigen for LECs from Group A, which only received the second immunization, and Group C, which received both immunizations. Consistent with our previous results (Fig. 1), the LEC subsets with the highest levels of antigen in the dual vaccinated mice (Group C) are cLECs, fLECs, and collecting LECs (Fig. 4B). As expected, we also observed minimal background levels of the BC#2 antigen for mice that did not receive the BC#2 immunization (Fig. 4B, C). Comparison of the BC#2 antigen levels for single vs dual immunized mice (Group A vs Group C) revealed elevated levels of archived antigen in mice that received both the BC#1 and BC#2 immunizations 42 and 21 days prior to euthanasia (Group C) (Fig. 4B–D). This suggests that LECs that previously archived antigen are able to acquire and/or retain more of a second antigen. Whether this function of increased antigen archiving is permanent and the result of an altered transcriptional program caused by antigen acquisition or inflammation is still unclear.

Using this dual immunization model, we next tested the inverse scenario and asked how successive immunizations affect retention of previously archived antigen. To do this we compared levels of the BC#1 antigen for mice that only received the first immunization (Group B) vs mice that received both vaccinations (Group C) (Fig. 4A). Similar to the results for the BC#2 antigen, we saw significantly higher levels of the BC#1 antigen in dual immunized mice, suggesting prolonged retention of the previously archived antigen (Fig. 4E−G, S6A). Taken together, these results indicate that sequential vaccinations promote an overall increase in antigen archiving by LECs.

To further investigate the dynamics of antigen uptake and retention, we next asked whether increased antigen levels observed in dual immunized mice was due to distinct groups of LECs acquiring each antigen. Evaluation of LECs from the 42 day time point indicated a substantial fraction of cells with low levels of antigen that expressed a gene program predictive of increased antigen archiving ability (Ag-competent, Fig. 2B). This represents a cell population that could be well suited to take up new antigen during a future immune challenge. From this observation, we predicted that in dual immunized mice we would observe two distinct groups of Ag-high cells, one primarily containing antigen from the first immunization (BC#1) and a separate group containing antigen from the second immunization (BC#2). To test this model, we compared levels of each tagged antigen in the dual immunized mice. Contrary to our prediction, we did not observe distinct groups of LECs that exclusively archived the different antigens, but instead found a strong correlation between levels of the tagged antigens for each LEC subset, with cells containing high levels of the first antigen (BC#1) also showing high levels of the second antigen (BC#2) (Fig. 4H, S6B). We confirmed these findings in vivo using flow
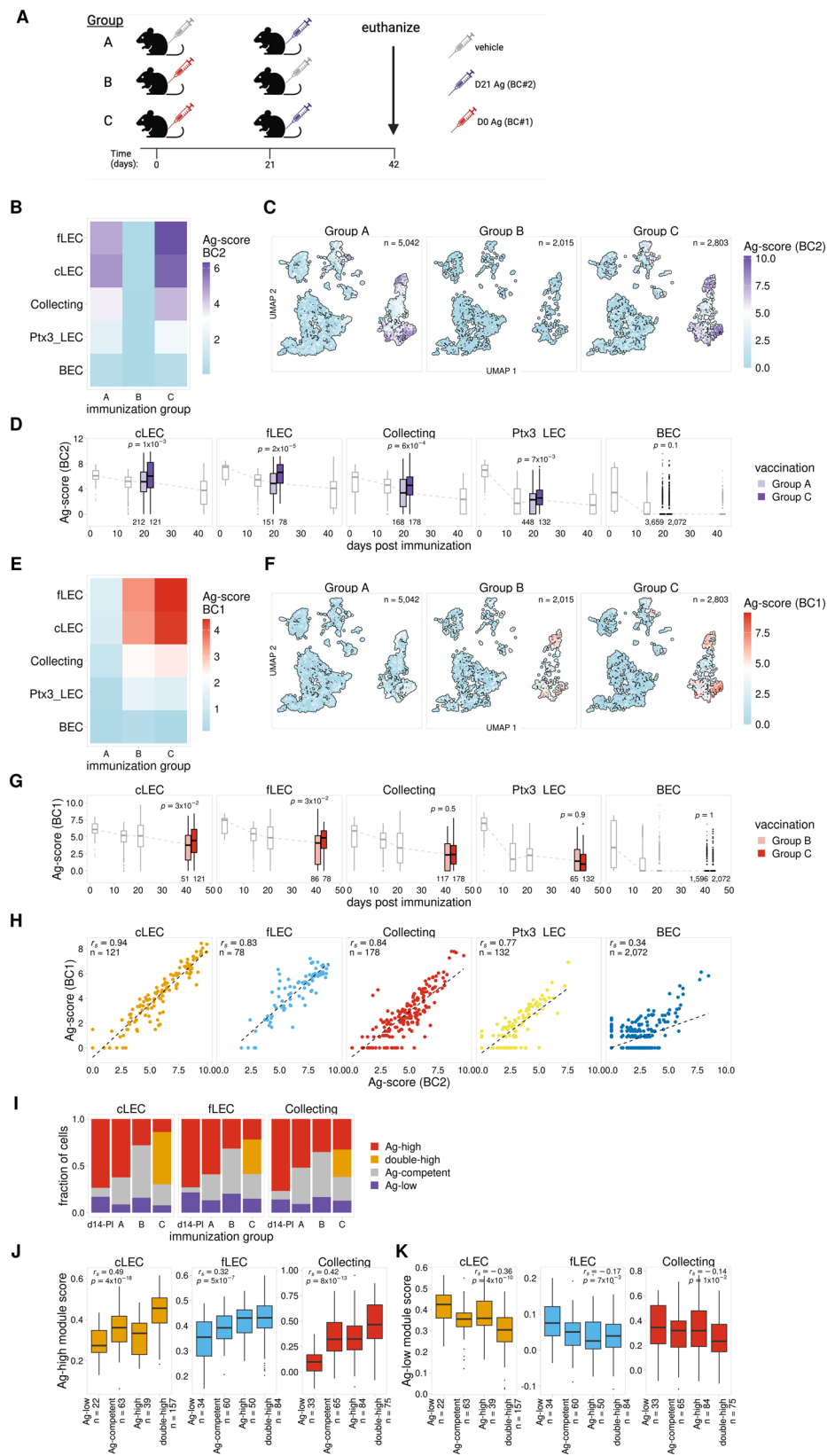
cytometry of fluorescently labeled ovalbumin with polyI:C/aCD40, and similarly found that the same LECs from draining LNs of mice immunized 1 week apart were positive for both antigens delivered sequentially (Figure S6C), indicating there are populations of cells within each LEC subset that are particularly well suited to archive antigen and will acquire antigens from repeated immune challenges.

Finally, we next asked whether there were distinct gene expression signatures associated with cells that archived multiple antigens in the dual immunized mice. We analyzed expression of the previously identified Ag-high and Ag-low gene modules (Fig. 2, Supplementary data 2) to determine if these programs might also influence the ability of an LEC to archive antigens from multiple immunizations. We

identified LECs from the dual immunized mice that had high levels of each antigen using the antigen score cutoffs derived from the day 14 time point (Fig. 2A) and predicted Ag-competent cells using our previously described classification models (Fig. 2, S4, Supplementary data 1). We then identified LECs with high levels of both antigens (double-high), high levels of only one antigen (Ag-high), low levels of both antigens but predicted to be Ag-competent (Ag-competent), and low levels of both antigens (Ag-low). We found that the fraction of predicted Ag-competent cells decreases in the dual-immunized sample (Group C), suggesting that the predicted Ag-competent cells become Ag positive cells after a second immunization (Fig. 4I). Comparison of these groups reveals a significant correlation with expression of the Ag-high and Ag-low gene programs (Fig. 4J, K, S6D, E). The double-high cells, which are the most proficient at archiving, had the highest expression of the Ag-high gene program and the lowest expression of the Ag-low gene program for each LEC subset (Fig. 4J, K, S6D, E). These findings suggest that we have identified at least some of the gene programs that promote antigen archiving during an initial immunization and that these programs also function to promote archiving during sequential immune challenges.

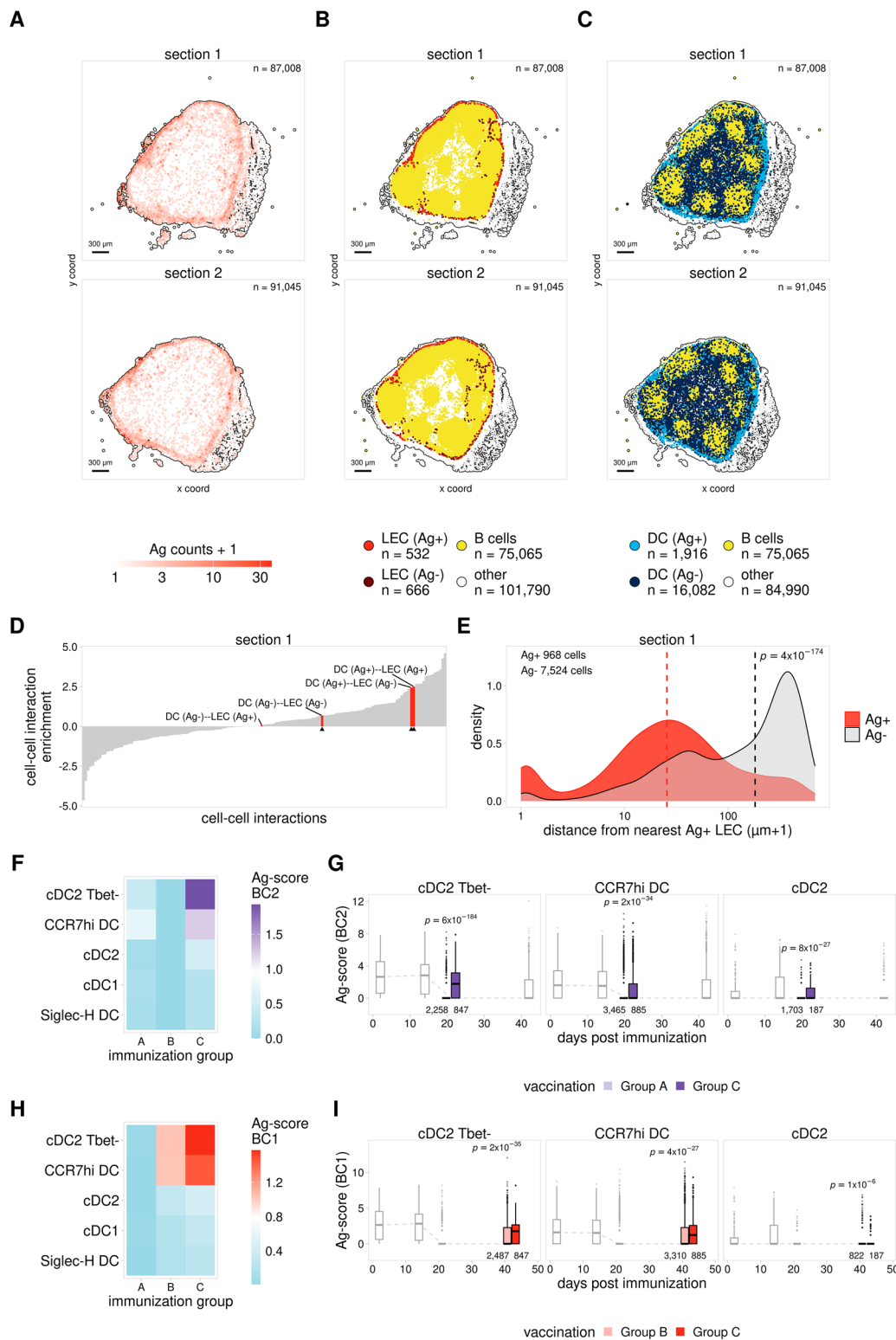## Antigen exchange with DCs correlates with levels of antigen archiving

We have previously shown that to enhance protective immunity, LECs exchange archived antigen with migratory DCs, which present to memory CD8 + T cells[9,10]. To further investigate antigen exchange between LECs and DCs, we assessed the spatial localization of antigen in the dLN using two spatial transcriptomics platforms, Xenium (10x Genomics) and GeoMx DSP (Nanostring). We repeated our dual vaccination experiment and immunized mice with OVA-psDNA 21 days prior, 42 days prior, or sequentially 21 days apart using OVA-psDNA conjugates containing unique barcodes with VV (Fig. 4A). We excised draining popliteal LNs at each time point, fixed with formalin, and embedded into paraffin. Tissue sections were cut and analyzed with the Xenium and GeoMx DSP platforms using probes for the mouse transcriptome and custom probes recognizing the antigen barcodes and genes associated with specific LEC subsets.

To classify cell types present in the 10x Xenium sections we generated a reference based on the cell type annotations from our scRNA-seq data (Figure S2A) and compared this to expression patterns for the mouse genes included in our Xenium probe panel (see Methods). Using this approach we identified large populations of B cells, T cells, and DCs, along with smaller populations of stromal cells including LECs, BECs, and fibroblasts (Figure S7A). We further classified LEC subsets within the Xenium sections (cLEC, fLEC, Ptx3 LEC, Marco LEC, tzLEC). Shown are lymph node sections from Group B and Group C (Fig. 4A) showing the subcapsular sinus and medullary sinus regions identified by morphology (Figure S7B). The lymph node sections are named based on predominant morphology (eg subcapsular sinus or medullary sinus) (Figure S7). As previously described, medullary sinus lymphatics include Ptx3 and Marco transcripts[14], however, there is overlap in marker expression within these sections where Ptx3 and Marco cannot distinguish between cortical and medullary and Marco expression is overlapping with fLECs (Figure S7B). Regardless, analysis of antigen probe counts indicated that samples from mice receiving a single immunization showed only low levels of antigen (Figure S7C-E, Group A and B). To characterize cells harboring antigen, we next used the LN sections from immunized samples and classified Ag+ cells as any cell with at least 1 antigen count from the antigen probes. From this analysis, we find that LECs show the strongest enrichment of Ag+ cells (Fig. 5A, S7D) and that the Ag+ cells are over-represented in the subcapsular sinus compared to the medullary sinus of the lymph node (Figure S7E). Consistent with our previous findings, LN sections from mice that received both immunizations showed enhanced antigen signal that was specifically localized to the subcapsular sinus (Fig. 5A, S7D, E). This supports our previous scRNA-seq results showing that LEC populations making up the ceiling and floor of the subcapsular sinus (cLECs and fLECs) contain the highest levels of archived antigen (Fig. 1D–F).

We next asked, in the subcapsular sinus LN where we detected substantially more Ag, whether the localization of DCs to different regions of the LN influenced the amount of antigen acquisition by DCs. Assessment of the localization of Ag+ and Ag- DCs within the dual immunized sample shows that Ag+ DCs localize in and around the lymphatic sinus, while Ag- DCs are broadly distributed throughout the LN (Fig. 5C). To further quantify this result, for each DC we calculated both cell proximity enrichment, and the distance to the closest Ag+ LEC. We found that Ag+ DCs showed enrichment of cell-cell interactions with Ag+ LECs, while Ag- DCs showed no significant enrichment of interactions with Ag+ LECs, we did not distinguish between subcapsular and medullary sinus in this analysis (Fig. 5D, S7F). Furthermore, Ag+ DCs are localized in significantly closer proximity to Ag+ LECs than Ag- DCs (Fig. 5E, S7G). This observation supports our previous results[8,9], and suggests that antigen archived by LECs in the lymphatic sinus is handed off to DCs located near the lymphatic sinus or passing through the lymphatic sinus.

The close proximity of Ag+ LECs and DCs is further supported by analysis of the single and dual immunized samples (Fig. 4A) using the

Fig. 5 | Antigen exchange with DCs correlates with levels of antigen archiving.
A Antigen counts are shown for adjacent LN tissue sections from a dual-immunized mouse analyzed with the Xenium platform. **B** Localization of Ag+ and Ag- cells is shown for LECs for tissue sections from (**A**). **C** Localization of Ag+ and Ag- cells is shown for DCs for tissue sections from (**A**). **D** Cell-cell interaction enrichment results are shown for section 1 from A for Ag +/- LECs and DCs. Red bars indicate LEC-DC interactions, arrows indicate significant enrichment for LEC-DC interactions, interactions between other cell types are shown as grey bars. **E** The distance to the closest Ag+ LEC is shown for Ag+ and Ag- DCs for section 1 from (**A**). **F** Mean day 21 (BC2) Ag-score is shown for DCs from mice that received a single immunization (day 21-Group A) or dual immunization (day 0 and day 21-Group C). **G** Ag-

score is shown for single and dual immunizations for the 21 day timepoint (BC2) for DC subsets with the highest Ag-score. Other timepoints are shown in grey. *P*-values were calculated using a one-sided Wilcoxon rank sum test with Benjamini-Hochberg correction. Values are shown for one biological replicate, a second biological replicate is shown in Figure S8. Each "biological replicate" contains cells from 8 mouse LNs pooled. The center line, box limits, whiskers, and points represent the median, interquartile range (IQR), the range within 1.5×IQR from the box limits, and points outside this range (outliers), respectively. **H** Mean day 0 (BC1) Ag-score is shown for DCs from mice that received single or dual immunization as described in (**F**) except for Group B and C. **I** Ag-score is shown for single and dual immunizations for the day 0 timepoint as described in (**G**) except for BC1.

GeoMx DSP platform where we evaluated subcapsular and medullary sinus as well as cortical lymphatic regions. For these samples, we obtained GeoMx data for a total of 15 individual LNs divided across two slides (Figure S8A). Distinct regions (composed of >500 cells on average) within each dLN were selected for analysis, including the SCS, medullary sinus, and cortex (Figure S8B). The GeoMx platform allows each selected region to be further segmented based on fluorescent staining. To distinguish between different cell populations, each region was segmented based on antibody staining for LYVE-1 (LECs), CD11c (DCs), and CD4 (T cells) (Figure S8B).

To identify regions with the highest levels of antigen, we next compared the normalized antigen signal for antigen probes. We then scaled the normalized signal separately for each antigen probe. We found that antigen levels for both Lyve-1+ and CD11c+ segments are highest within the SCS regions with significantly less antigen in the cortex and medullary regions (Figure S8C) consistent with our single cell data showing a sharp decline in cortical/medullary lymphatics (Ptx3/Marco) (Fig. 1). In addition, there was a strong correlation between antigen signals for Lyve-1+ and CD11c+ segments within each region, and regions with higher antigen levels in LECs (LYVE-1 +) also showed higher antigen levels in DCs (CD11c +) (Figure S8D). Taken together, our spatial transcriptomics results (Fig. 5A–E, S7,S3) suggest that the amount of antigen exchanged with DCs is directly dependent on the amount of antigen archived by proximal LEC populations where lymphatic sinus LECs archive the most antigen and therefore DCs located near the sinus also have high amounts of antigen.

We next asked if there was increased antigen uptake by DCs in dual immunized mice, which showed higher levels of archived antigen in LEC populations (Fig. 4A–G, S6A). Due to the poor antigen signals obtained for single-immunized mice analyzed with the Xenium platform (Figure S7C), and the low number of regions obtained for dual immunized mice analyzed with the GeoMx platform (Figure S8A-D), we were not able to compare DC antigen signals using these spatial transcriptomics approaches. Instead, we used our scRNA-seq data to analyze DC populations from single- and dual-immunized mice (Fig. 4A). In support of our previous results (Fig. 1H–J), we found that CCR7^{hi} and cDC2 Tbet- populations had the highest antigen levels in the dual-immunized samples. In addition, similar to LECs (Fig. 4B–G,S6A), we found that DCs from dual immunized mice had significantly higher antigen levels than mice that only received one of the immunizations (Fig. 5F–I, S8E, F), suggesting DCs may also be predisposed during a second immune challenge to acquire more Ag. Furthermore, a second immunization led to increased Ag from the first immunization in some DC subsets (Fig. 5I, S8F). These results in conjunction with our spatial transcriptomics data (Fig. 5A–E, S7), support a model wherein successive vaccinations enhances antigen uptake and archiving, which in turn results in increased exchange of antigen with proximal or migrating DC populations.

Antigen archiving is impaired following CHIKV inoculation

Using the classification models trained for the main Ag+ LEC subsets, we identified cells that are predicted to be archiving-competent (Ag-competent) based on the expression of distinct gene programs (Fig. 2, Supplementary data 2). To further test the utility of these models, we asked if we could predict differences in the antigen archiving capability of LECs from naive mice and mice infected with CHIKV, which we previously reported impairs LN LEC antigen acquisition[16]. We used previously published scRNA-seq data of murine LNSCs 24 h after infection with the arthritogenic alphavirus CHIKV[16,17]. CHIKV infection in mice disrupts the structure and function of the draining lymph node[17,20] and induces a proinflammatory and antiviral response in LECs[16]. Importantly, by 72 h post-inoculation with WT CHIKV, antigen acquisition by LN LECs is impaired[16]. Using scRNA-seq data for LNSCs at 24 h post CHIKV inoculation (Fig. 6A), we asked if we could use our antigen archiving classification models to demonstrate whether CHIKV

inoculation would also impede antigen archiving of antigens administered at 24 h post inoculation.

The scRNA-seq data of endothelial cells from CHIKV-inoculated mouse LNs includes similar subsets of LECs, including cLECs, fLECs, and collecting LECs (Fig. 6A). To evaluate antigen archiving during CHIKV infection, we predicted archiving ability for cLECs, fLECs, and collecting LECs from mock- and CHIKV-inoculated samples using the classification models previously trained for each of these subsets (Fig. 6B, C, S9). To first assess the accuracy of these predictions, we compared expression of the Ag-high and Ag-low gene modules derived from each model (Fig. 2, Supplementary data 2). As expected, there was overall higher expression of the Ag-high gene module for LECs predicted to be archiving-competent (Ag-competent) (Figure S9A). We next compared the fraction of Ag-competent cells for the mock- and CHIKV-inoculated samples. We found that for the combined population of antigen archiving LECs (cLECs, fLECs, collecting LECs), there was a significant reduction in the overall fraction of Ag-competent cells for CHIKV-inoculated mice (Figure S9C), with cLECs showing the largest reduction using 2 independent models (Fig. 6B, C, S9D). Comparison of expression differences for the Ag-high and Ag-low gene modules for mock- and CHIKV-infected mice further supported these findings. For cLECs we found a significant reduction in expression of the Ag-high module and an increase in expression of the Ag-low module during CHIKV infection (Fig. 6D–F, S3B). However, fLECs and collecting LECs both had less pronounced changes in the fraction of Ag-competent cells and in the expression of these modules. fLECs showed some increase in Ag-competent cells and a corresponding increase and decrease in the Ag-high and -low modules, respectively, while collecting LECs only showed subtle differences in the expression of each. These results suggest an overall reduction in antigen archiving ability at 24 h post infection.

CHIKV inoculation limits antigen archiving

To experimentally test the prediction that CHIKV inoculation disrupts antigen archiving, we inoculated mice in the footpad with PBS (mock) or 10^3 PFU of WT CHIKV[16]. After 24 h, CHIKV and mock injected mice were injected with 10 µg OVA-488 in both calf muscles, and OVA-488^{+} LECs were evaluated in the dLN 17 days later. As a positive control, mice were immunized with 10 µg OVA-488, 5 µg polyI:C and 5 µg αCD40 in each hind limb. There was a significant reduction in the percentage and number of OVA-488+ LECs in mice inoculated with WT CHIKV or mock when compared with OVA-488/polyI:C/αCD40 immunized mice (Fig. 7A, B, S1B). Notably, there was a significant reduction in the percentage of OVA-488+ LECs in WT CHIKV inoculated mice compared with mock infected mice (Fig. 7A, B). To further assess whether the OVA archived antigen was functionally active and presented by DCs we adoptively transferred in OVA specific TCR transgenic OT1 CD8 + T cells labeled with violet proliferation dye (VPD) and calculated the percent of OT1s divided (Fig. 7C, S1B). Like the reduction in fluorescent antigen detected within the LECs, we observed significantly less OT1 division in mice inoculated with WT CHIKV prior to OVA-488 injection (Fig. 7C). Thus, these findings support the accuracy of our predictive models and further demonstrate how gene expression patterns can be used to inform LEC antigen archiving capability.

Human LN LECs acquire and retain foreign antigen

Using predictive models we evaluated antigen archiving potential in mice that were not immunized with our antigen-psDNA conjugates (Figs. 6, 7, S9). We next sought to further assess the portability of these models (Figs. 2, S4, 5, Supplementary data 2) by applying them to human datasets. To do this, we utilized previously published human scRNA-seq data for follicular lymphoma samples (FL) and metastasis-free control LN samples (MFLN)[47]. We first annotated LEC subsets using human reference data[48] and were able to identify LEC subsets described previously[48] (Figure S10A). To assess antigen archiving, we
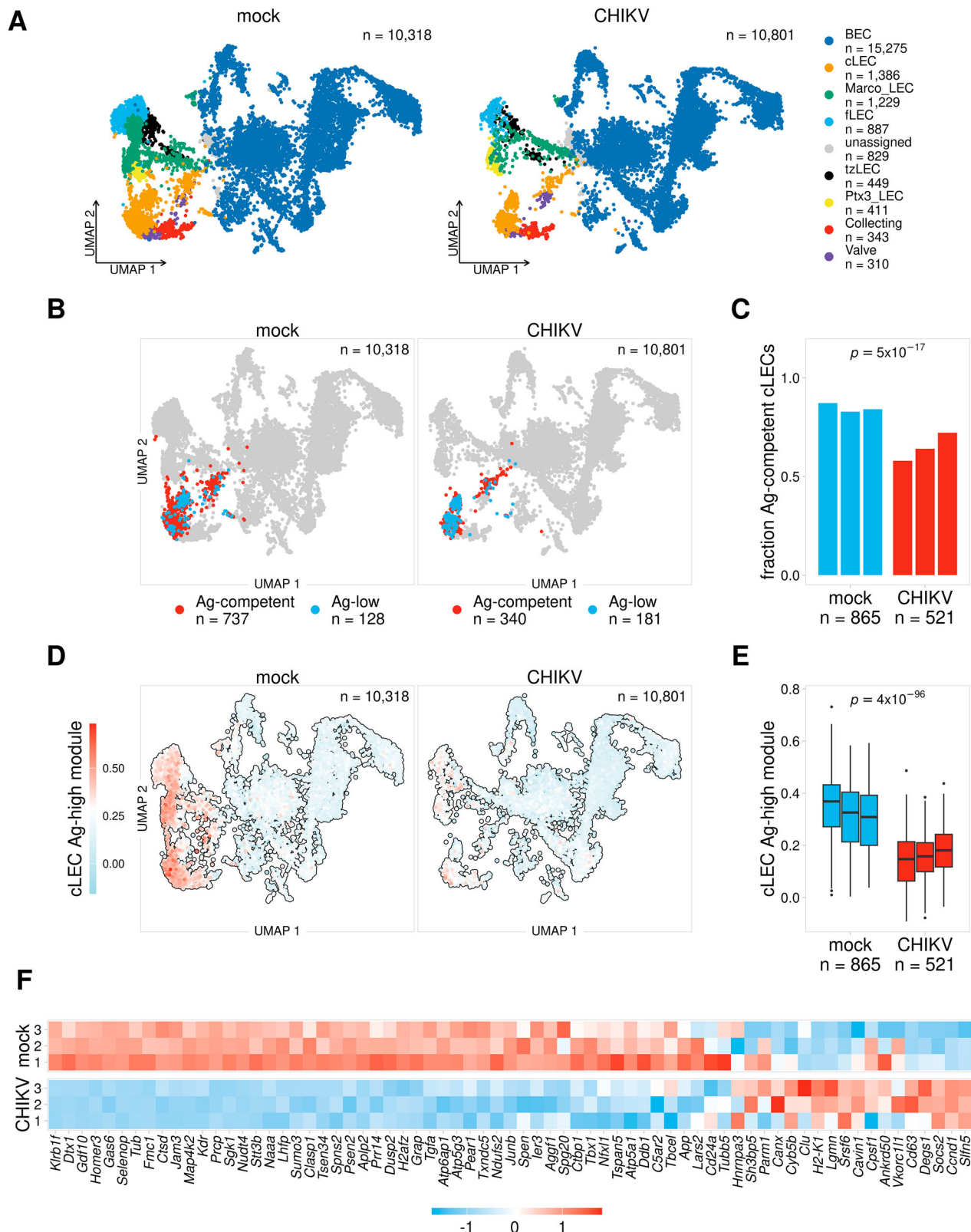
Fig. 6 | Antigen archiving module predicts reduced antigen archiving during CHIKV infection. A UMAP projections show LEC subsets for mock and CHIKV-infected mice ($n = 3$ biological replicates, cell numbers are included on UMAP). B UMAP projections show predicted Ag-competent cLECs for mock and CHIKV-inoculated mice after 24 hours. C The fraction of predicted Ag-competent cLECs is shown for mock and CHIKV-inoculated mice for each biological replicate ($n = 3$). P-values were calculated using a two-sided Fisher's exact test with Benjamini-Hochberg correction for all replicates pooled together. D UMAP projections show

cLEC Ag-high module scores for mock and CHIKV-inoculated mice. E cLEC Ag-high module scores are shown for mock and CHIKV-inoculated mice for each biological replicate. P-values were calculated using a two-sided Wilcoxon rank sum test with Benjamini-Hochberg correction. The center line, box limits, whiskers, and points represent the median, interquartile range (IQR), the range within 1.5×IQR from the box limits, and points outside this range (outliers), respectively. F Relative expression of the top 70 genes from the cLEC Ag-high gene module is show for mock and CHIKV-inoculated mice for cLECs from three biological replicates.

identified human homologs for our antigen archiving gene programs (Fig. 2, S4, Supplementary data 2). We then used the cLEC, fLEC, and collecting LEC models to predict antigen-archiving competent (Ag-competent) cells for each respective population. We found that the fraction of Ag-competent cLECs, fLECs and collecting LECs (-0.5–0.75) was similar to what we observed in mice (Figs. 5C, 7D–F, S9C, D, S10B, C) irrespective of the predictive model used. Comparison of MFLN and FL samples predicted similar fractions of Ag-competent cells, suggesting that follicular lymphoma may not affect the archiving ability of cLECs (Fig. 7D–F) or fLECs and collecting LECs (Figure S10B,

C). To better evaluate the capacity of human LN LECs to acquire and retain foreign antigen we next tested a human LN explant model. Human pancreatic LNs acquired from deceased donors (Supplementary Data S4), were cut into thirds and placed into media. LN pieces were then treated with OVA-488 or OVA-488+polyI:C overnight and then washed and placed into new media without OVA-488/polyI:C. The same day (day 1) or two days later (day 3) LNs were digested and stained for flow cytometry to assess antigen levels within LECs (Fig. 7G, S1C). We found that LECs had a high percentage of antigen positive cells at both day 1 and day 3 after treatment (Fig. 7G, H) and addition of

Fig. 7 | Antigen acquisition and archiving after chikungunya virus (CHIKV) inoculation and in human lymph nodes (LN)s. A Mice were infected with 10^3 PFU of WT chikungunya virus (CHIKV) or mock inoculated (PBS) 1 day prior to administration of 10 μg OVA-488 or OVA-488/polyI:C/αCD40 (10 μg/5 μg/5 μg). 17 days later mice were euthanized and dLNs were extracted and processed for flow cytometry. Shown are representative flow plots gated on LECs (CD45-CD31 + PDPN +). Intracellular adhesion molecule 1 (ICAM1)xovalbumin alexa fluor 488 (OVA-488) is shown. **B** Quantification of mouse groups in A showing percent of OVA-488 positive lymphatic endothelial cells (LEC)s and number of OVA-488 positive LECs. Each dot represents 2 dLNs from 2 pooled mice ($n = 6$/group) except OVA-488/polyI:C/αCD40 which is 2 dLNs from 1 mouse injected in both footpads ($n = 5$) and naïve $n = 4$. Experiment was repeated on two independent occasions. OVA only vs WT CHIKV OVA *$p = 0.0441$, OVA only vs naïve *$p = 0.0307$, ****$p < 0.0001$, ns is $p > 0.05$ by one-way ANOVA with Tukey's two-sided multiple comparison test. Data are presented as mean values +/- SEM. **C** Violet proliferation dye (VPD) labeled OT1 CD8 + T cells were transferred into mice described in A at day 14. At day 17 transferred OT1 T cells in dLNs were gated as (CD8 + CD45.1 +). Proliferation (percent divided OT1) was calculated based on VPD dilution. Each dot represents 2 dLNs from 2 pooled mice ($n = 6$/group) except OVA-488/polyI:C/αCD40 which is 2 dLNs from 1 mouse injected in both footpads ($n = 5$) and naïve $n = 4$. All data points are shown. Experiment is combined data from two or more experiments. Adjusted *p*-values are as follows: OVA/polyI:C/αCD40 vs OVA only ***$p = 0.0002$; OVA only vs WT CHIKV OVA *$p = 0.0111$; OVA only vs naïve *$p = 0.0403$, ****$p < 0.0001$, by one-way ANOVA with Tukey's two-sided multiple comparison test. **D** The fraction of ceiling LECs predicted to be antigen competent is shown for each metastasis-free lymph node (MFLN-teal) and follicular lymphoma (FL-red) LN sample with at least 20 identified cLECs. **E** The median fraction of predicted antigen-competent cells is shown for samples from (**D**). Points show values for each sample. *P*-values were calculated using a two-sided Wilcoxon rank sum test with Benjamini-Hochberg correction. **F** The median fraction of predicted antigen competent cells is shown for a second independent model as in (**E**). Points show values for each sample. *P*-values were calculated using a two-sided Wilcoxon

rank sum test with Benjamini-Hochberg correction. **G** Human pancreatic LN pieces were treated overnight with 5 μg/mL of OVA-488 and 2.5 μg/mL Poly I:C, 5 μg/mL OVA-488 alone, or PBS (no treatment). LNs were digested, stained, and gated on LECs (CD45-PDPN + CD31 +). Shown are representative flow cytometry plots as in (**A**). **H** Quantification of percent OVA-488 + LN LECs 1 or 3 days after overnight treatment described in (**G**). Each dot represents 1 LN piece. All data points are shown. no treatment (NT) d1: $n = 12$, ova488 d1: $n = 9$, OVA-488 polyI:C d1: $n = 11$, NT d3: $n = 13$, OVA-488 d3: $n = 11$, OVA-488 polyI:C d3: $n = 14$. Experiment was repeated on 2 independent occasions for OVA-488 d1 and 3 independent occasions for all other samples except NT and OVA-488 polyI:C d3 which were performed on 4 occasions. Each occasion represents 1 deceased donor. ns is $p > 0.05$, OVA vs NT d3 adjusted *$p = 0.0116$, OVA polyI:C vs NT d3 adjusted ***$p = 0.0003$, ****$p < 0.0001$ by one-way ANOVA with Tukey's two-sided multiple comparison test. Data are presented as mean values +/- SEM. **I** Quantification of percent OVA-488 + LN BECs (CD45-PDPN-CD31-) 1 or 3 days after overnight treatment described in (**G**). Each dot represents 1 LN piece. All data points are shown. Sample numbers and replicates are exactly as in (**H**). ns is $p > 0.05$, OVA polyI:C vs NT d3 adjusted **$p = 0.0048$ and OVA polyI:C vs NT d3 adjusted **$p = 0.0014$ by one-way ANOVA with Tukey's two-sided multiple comparison test. Data are presented as mean values +/- SEM. **J** Quantification of percent OVA-488 + LN fibroblastic reticular cells (FRC)s (CD45-PDPN + CD31-) 1 or 3 days after overnight treatment as described in (**I**). Each dot represents 1 LN piece. All data points are shown. Sample numbers and replicates are exactly as in (**H**). Ns= $p > 0.5$ where NT vs OVA-488 d3 $p = 0.0705$ by one-way ANOVA with Tukey's two-sided multiple comparison test. Error bars indicate standard error of the mean. **K** Quantification of percent OVA-488 + LN classical monocytes (CD45 + CD19-HLA-DR + CD14 +) 1 or 3 days after overnight treatment as described in (**I**). Each dot represents 1 LN piece. All data points are shown. Sample numbers and replicates are exactly as in (**H**). ns is $p > 0.05$, NT vs OVA-488 d1 adjusted *$p = 0.0361$, NT vs OVA polyI:C d3 adjusted **$p = 0.0047$, adjusted ****$p < 0.0001$ by one-way ANOVA with Tukey's two-sided multiple comparison test. Data are presented as mean values +/− SEM.

polyI:C resulted in significantly higher levels than corresponding no treatment controls (Fig. 7H), similar to our animal models (Fig. 7A–C). Among the other LNSC populations evaluated we observed some BECs (Fig. 7I) and FRCs (Fig. 7G) with antigen, particularly at the day 3 timepoint. We also evaluated CD45+ cells and observed the highest amount in HLA-DR + CD14+ classical monocyte populations, although we were unable to fully assess all myeloid cell populations (Figure S1C). Overall these results illustrate the utility of our approach to investigate antigen archiving in human samples and suggests that antigen archiving by LECs may be a process conserved across species.

Discussion

In this study, we defined a gene signature associated with LEC antigen archiving using an antigen conjugated to a DNA tag for use with scRNA-seq. LECs acquire and archive foreign antigens beyond the peak of the primary immune response[8–11]. We previously demonstrated that antigen can be detected using a psDNA tag conjugated to a protein antigen for up to 14 days post-immunization, using single cell sequencing[11]. We further extended this timeline to 21 and 42 days post-immunization to assess the temporal dynamics of antigen archiving. Corroborating our published data, we found that antigens persist predominantly in LEC subsets, such as cLEC, fLEC, and collecting LEC, at late time points following both single and dual immunizations (Figs. 1F, 4D, G). Notably, Ptx3 LECs capture antigens at day 2, but by day 14 antigen levels decline in these cells. One potential explanation for the loss of antigens within the Ptx3 LEC subset may be the lack of expression of *Cd274* (PDL1). PDL1 is an important regulator of LEC division and survival where loss of PD-L1 leads to increased LEC division[49]. Indeed, the LECs that undergo division during LN expansion following immunization are also the LECs that undergo apoptosis[49]. Thus, Ptx3 LECs, which have low expression of *Cd274*[14], likely undergo apoptosis and lose antigens earlier than the other LEC subsets during LN contraction.

Furthermore, we trained machine learning models to predict cells capable of antigen archiving. The training of these classification models was based on the day 14 time point because it was an intermediate time point with robust antigen high and low cell populations. As a proof of concept, these models were able to predict the decrease in Ag-competent cells following CHIKV infection. Extensive data[16] demonstrate how CHIKV infection disrupts the organization of the LN through interactions with LNSCs. We further tested the accuracy of these predictions by assessing the ability of LECs to archive fluorescent antigens in CHIKV-inoculated mice (Fig. 7A–C). Thus, these classification models are an important advancement, as they enable the analysis of antigen archiving competency in existing and future scRNA-seq datasets from different infections, immunizations, or disease states. This could be particularly important to identify which infections or inflammatory stimuli promote or hinder antigen archiving and could inform studies regarding when or which area to vaccinate. Upon expanding on our published study using antigen-DNA conjugates as a molecular tracking system, we demonstrated that the incorporation of two different antigen tags can accurately model the kinetics of antigen signals in different cell types using scRNA-seq. Furthermore, the generation of machine learning models to assess antigen archiving presents a unique approach for future applications.

Genes associated with endosomal-lysosomal function were captured as part of this antigen archiving gene signature. Lysosomal-associated genes in the Ag-high module (Figure S4B) could result from the large amount of antigen within the LECs. It seems likely that LECs trap foreign antigens as they pass through the LN similar to how LECs capture viral particles to prevent viral dissemination[17]. Ultimately, LECs must degrade or release antigens to neighboring cells, such as DCs. Antigen exchange between LECs and DCs causes small amounts of DC antigen presentation over a limited time period, which is likely an evolutionary benefit. Indeed, we have previously demonstrated an increased capacity for DC presentation of archived antigens during an

unrelated infection[8]. During infection, the increased activation state of the DCs that acquire both antigens from the infection and antigens from LECs leads to improved memory T cell responses and increased effector function[8]. LECs acquire antigens via different endocytic pathways. We demonstrated that LEC endocytosis of proteins occurs via caveolin and clathrin mediated endocytosis (Fig. 3). Interestingly, caveosomes maintain a neutral pH and cargo can remain in caveosomes until transcytosis/recycling or lysosomal degradation via RAB5 dependent fusion with the early endosome[50]. Here we more specifically tested if caveolin is an important mediator of antigen archiving. Indeed, loss of *Cav1* increases antigen degradation in vivo. Our data provided in Fig. 3 demonstrates that individual genes associated with the antigen archiving gene signature are part of the process by which antigen archiving is programed. Perhaps even more interesting is the limited difference in antigen archiving resulting from the loss of caveolin mediated endocytosis. These findings highlight that multiple genes contribute to the process of antigen archiving and elimination of just one gene or pathway may not be enough to disrupt the cellular process of antigen archiving. Furthermore, the data presented here suggest that specific LECs are "pre-coded" to be competent in antigen archiving, particularly when our classification models were applied to naïve mice (Fig. 6, S4D, E). These models predict that certain LECs within naïve mice are predisposed to express the antigen-archiving gene signature (Figure S4D, E, S9C, D).

As LECs do not directly present archived antigens to CD8 T cells, there is a need for antigen exchange from LEC to migratory DC for the presentation of archived antigen-derived peptides[8,9,11]. Indeed, antigen-bearing LECs interact, particularly those that express ICAM1, and exchange antigen with DCs[9]. Building upon the live imaging of LEC-DC interactions to exchange archived antigens[9], here we visualized the spatial localization of antigen bearing cells in the LN using the 10X Genomics Xenium and Nanostring GeoMx platforms. We confirmed by scRNA-seq that antigen signals within LEC and DC subsets correlated with our spatial data. We found that CCR7hi DCs and cDC2 T-bet- DCs had antigen levels peaking at 14 days post-immunization and that antigen levels dramatically decreased by day 21 post-immunization (Fig. 1J). Interestingly, when we further extended this time course to 42 days, we still detected antigens in cDC2 Tbet- and CCR7hi DC populations (Fig. 1J). While it is unlikely that DCs are still acquiring and processing antigens from the initial immunization several weeks earlier, this finding supports the hypothesis that LECs are slowly releasing antigens over time through either direct LEC-DC interactions or via LEC apoptosis. Importantly, the amount of antigen within LECs may directly correlate with the effector T cell response. As we have previously published[9] and demonstrate here following CHIKV infection (Fig. 7A–C), antigen specific T cell responses correlate with amount of antigen detected within LECs. Indeed, in our immune challenge studies we find that only during the duration of antigen archiving when we see robust OT1 division (3 weeks) versus no OT1 division (8 weeks) do we observe an increased benefit in T cell mediated local protection against a pathogen expressing the archived antigen[8].

In dual-immunized mice, cLECs, fLECs, and collecting LECs have enhanced antigen acquisition and retention compared to mice receiving a single immunization (Fig. 4D, G, S6A). The data we provide suggest: *i.* that LECs are capable of acquiring multiple antigens and *ii.* that LECs that already acquired one antigen are more effective at acquiring a second antigen. We found that the gene signature for LECs following one immunization is similar to the gene signature of LECs with multiple archived antigens. This suggests there are LECs that are susceptible to being reprogrammed for antigen acquisition and archiving (Ag-competent). It is possible that LNSCs, particularly LECs, undergo epigenetic reprogramming during an initial antigen encounter that provides increased responsiveness in regard to antigen acquisition. Immune memory is thought to be mediated by epigenetic

changes, alterations in gene expression, and metabolic reprogramming within innate immune cells. These changes lead to a heightened state of readiness and elimination of pathogens upon subsequent exposure[51,52]. Interestingly, this memory is not limited to immune cells as one study showed that IFNb stimulation contributes to increased and quicker induction of interferon-stimulated genes (ISG) in mouse embryonic fibroblasts[53]. Upon restimulation, the rapid induction of ISGs was attributed to increased recruitment of RNA polymerase II to ISG loci and this was also associated with H3.3 and H3K36ME3 marks on the chromatin of ISG genes[53]. Thus, it is possible that LECs may undergo epigenetic modifications upon antigen acquisition to promote subsequent antigen uptake and retention.

We found higher antigen levels in both LEC subsets and DC subsets, CCR7hi DC and cDC2 Tbet-, upon a second antigen exposure when compared to single-immunized mice (Fig. 4D, G, S6A, C). This supports our published data demonstrating that migratory DCs[9] and cDC1s are required for cross-presentation of archived antigens during the time frame of LEC apoptosis[8]. We previously published that migratory DCs are important for archived antigen exchange resulting from both LEC apoptosis and direct LEC-DC interactions at late time points after immunization[54–57]. In this study we show that LEC-DC interactions within the subcapsular sinus region of the LN are indeed enhanced when either cell type contains the archived antigen (Fig. 5D, E, S7D, E). While early after immunization lymphatic sinus (LS) DCs acquire and process antigens in the medullary region[58] we detected much less antigen within the medullary sinus LECs as classified by transcriptional signature (Figure S2, Figure S7B, E) and location (Figure S7B, S8A, B) suggesting antigen transfer in this region is limited at late time points when the majority of the archived antigen is found within the floor and ceiling LECs rather than the cortical/medullary LECs (Ptx3/Marco) (Fig. 1, S7A–E, S8C). It is a unique finding that the cDC2 Tbet- DCs are positive for antigen following the dual immunization. Based on our prior findings we anticipated that CCR7hi DCs would be antigen positive after dual immunization as they migrate to the LN and interact with LECs. There are several possible explanations for why the cDC2 tbet- DCs are antigen positive after dual immunization including localization. Previously characterized LS DCs are CD11b+ DCs located in proximity to the LECs and CD169+ subcapsular sinus macrophages[58]. It is possible that the antigen we are detecting in our CD11b + cDC2 tbet- population are acquiring antigen resulting from direct LEC-LS-DC interactions and exchange. Another possibility is that the cDC2 tbet- population is derived from the CCR7hi DCs. As the CCR7hi DCs enter the cortex of the LN it is a possibility that they downregulate of CCR7 and become part of the cDC2 tbet- cell population. Alternatively, DCs may have higher levels of antigen after a second exposure for the same reason as LECs. Myeloid progenitor cell populations do undergo innate training and thus perhaps DCs are also capable of increased antigen acquisition in addition to increased cytokine release as has been described[51,59,60]. Future studies understanding how archived antigen bearing DCs differentiate are required to fully understand why both migratory and cDC2 Tbet- DCs are antigen positive at late timepoints.

A caveat to our spatial transcriptomics studies is our inability to directly compare antigen signals from single- and dual- immunized mice. However, the Xenium and GeoMx spatial transcriptomics platforms lack the depth of scRNA-seq, making antigen detection sparse and limited by the ability of the probe to bind the target. To address this limitation we coupled spatial methods with scRNA-seq datasets. Here, we found that LECs and DCs in the subcapsular sinus of the LN had the highest levels of antigen. These data support our finding that sequential vaccinations enhanced LEC antigen archiving and antigen exchange. Overall, this manuscript provides confirmatory evidence of our prior publications using transcriptional profiling and antigen-DNA tags. To build upon these data we provide a unique resource to assay antigen archiving capacity by identifying an antigen archiving gene

signature and generating an antigen competency model to predict outcomes from other datasets, including those derived from human samples. Indeed, our analysis suggests a similar gene expression program is expressed in human LEC populations from existing datasets[48], highlighting how processes like antigen archiving, defined in animal models of immunization, can be predictive of human biology. While difficult to completely address antigen archiving in human LNs we provide data here to suggest that LECs in the human LN perform similar endocytic function as LECs in a mouse LN. These findings are consistent with our predictions from human scRNA-seq data suggesting that LN LECs are antigen competent. Future studies are aimed at better defining the benefit of antigen archiving to humans and better understanding how LECs are programmed during immune responses to archive antigens.

Methods

All research complies with all relevant ethical regulations. All animal procedures were approved by the Institutional Animal Care and Use Committee at the University of Colorado under protocols 67 and 26. All human tissues were de-identified prior to distribution to our laboratory in line with the University of Colorado Institutional Review Board procedures and regulations. 3 male and 1 female deceased donor lymph nodes were used from donors ages 31–61 as indicated in source data and Supplementary data 4. All reagents, antibodies, dilutions and oligo sequences can be found below and listed in Supplementary data 5.

Statistics and Reproducibility

Each statistical test used to analyze data is indicated in the figure legends where p values were calculated. For animal and human LN experiments in Figs. 3 and 7 analysis was performed using FlowJo software version 10 (Tree Star Inc.) and GraphPad Prism version 10.1.1. Comparison of the means between samples were evaluated for statistically significant differences using a 1-way ANOVA test followed by a two-sided Tukey's multiple-comparison test. $P < 0.05$ was considered statistically significant. All analysis assumed both populations were normally distributed when parametric tests were used. A confidence interval of 95% was used. Each in vivo analysis was performed with 3–5 mice per group as determined by a power calculation using the assumption (based on prior data) that there would be at least a twofold change with a standard deviation of less than 0.5. To calculate numbers of animals to be used we performed a power calculation with an alpha of 0.5 and a 1-beta of 0.80 to determine at least 3 mice per group should be evaluated. Exact replicates and numbers are provided in the figure legends. Each analysis was done with at least three mice per treatment group and each experiment was done at least twice with the same results indicating reproducibility. A third replicate was not performed as our experiments were adequately powered to provide statistical significance in accordance with our IACUC policies regarding animal experiments with consistent data points. Error bars are mean ± the standard error of the mean.

Mice (mus musculus)

5–6 week-old C57BL/6 mice, *mus musculus*, (WT) were purchased from Charles River or Jackson Laboratory and bred and housed in the University of Colorado Anschutz Medical Campus Animal Facility. Housing conditions were as follows: Light cycle-14light,10dark; Temperature-72 degrees +/− 2 degrees Fahrenheit; Humidity: 40% +/− 10%; Water-hyperchlorinated (2–5 ppm) Reverse Osmosis delivered via automatic watering; Food-Teklad (Envigo) diets. The *Cav1^{fl/fl}* mice back crossed to C57BL/6 were received through material transfer agreement with University of Virginia School of Medicine through Dr. Brant Isakson. The *Prox1^{CreER-T2}* sperm was received through material transfer agreement from European Mouse Mutant Archive and rederived at the Genetically Engineered Mouse Models Core facility at

National Jewish Health and bred to *Cav1^{fl/fl}* at University of Colorado Anschutz Medical Campus Animal Facility. $n = 9$ mice were used per group where $n = 14$ males and $n = 22$ females were used at ~12 weeks of age. The major outcomes of CHIKV infection and antigen archiving in C57BL/6 mice are not influenced by biological sex. CHIKV inoculations were performed in 4 week old males. Female mice were used for Vaccinia virus experiments based on preferential viral replication in the ovary[61] at 6-8 weeks of age. OT1 mice were all bred on a C57BL/6 background. OT1 mice are a TCR transgenic strain specific to the SIINFEKL peptide of ovalbumin (OVA257-264) in the context of H-2K^b. Female or male OT1 mice were used for transfer experiments into either male or female mice were 1 OT1 was euthanized and 200-500 thousand donor OT1 were transferred from one mouse into multiple male and female recipients. Numbers of mice are indicated in the figure legends. No differences in antigen archiving or *Cav1* deletion between sexes in each group (see source data). Mice were euthanized with CO2 followed by cervical dislocation as a secondary method to confirm death.

Immunizations and Infections

6–8-week-old C57BL/6 (CD45.2) mice were immunized with 10^4 plaque-forming units (PFU) of Vaccinia Western Reserve or 5 μg of poly I:C (Invivogen) with or without 5 μg of anti-CD40 (FGK4.5, BioXcell) and 20 μg of OVA-psDNA or OVA in 50 μL volume per footpad injection. Endotoxin levels were quantified using the Pierce Limulus Amebocyte Lysate Chromogenic Endotoxin Quantitation kit (Thermo Scientific) to be less than 0.5 EU/mg for either OVA or OVA conjugated to psDNA. For CHIKV inoculations, 4 week old C57BL/6 mice were inoculated with 10^3 PFU of CHIKV AF15561 (WT CHIKV) in a 10 μL volume in both rear footpads.

Cre induction

Mice were injected intraperitoneally with tamoxifen in corn oil at 50 μg/gm four times, every other day. 1-2 weeks after the final tamoxifen dose mice were treated as described below except with 10 μg AF488-labeled ovalbumin, 5μg polyI:C, 5μg anti-CD40 per footpad and 2-17 days later LNs were removed and evaluated by flow cytometry using, anti-CAV1 (polyclonal, cell signaling) followed by donkey anti-rabbit secondary (poly4064-biolegend) and μLNSC stains outlined below.

Evaluation of antigen acquisition by flow cytometry

Antigen acquisition was evaluated using fluorescently labeled ovalbumin (OVA) as previously described[8–11,16]. Ovalbumin (A5503, Sigma-Aldrich) was decontaminated of lipopolysaccharide using a Triton X-114 detoxification method and tested with Pierce LAL chromogenic endotoxin quantitation kit (88282, Thermo Fisher Scientific). Ovalbumin was labeled using an Alexafluor 488 succinimidyl ester labeling system (A20100, Thermo Fisher Scientific). CHIKV-infected mice were inoculated with 20 μg AF488-labeled ovalbumin via intramuscular injection into both calf muscles (10 μg per calf) 24 h after virus inoculation. Fourteen days later Violet proliferation dye labeled OT1 T cells were transferred intravenously (~200,000) into immunized mice. Three days later popliteal LNs were collected for analysis of OVA^+ LNSCs and OT1 division by flow cytometry. As positive controls, mice were injected with 10 μg OVA-488 and 5 μg polyI:C, 5μg anti-CD40 per footpad. OT1 division was calculated as previously described in ref. 62 using the equation fraction diluted = $\sum_1^i N^i/2^i / \sum_0^i N^i/2^i$, where i is the generation number (0 is the undivided population), and N_i is the number of events in generation i.

For preparation of single-cell suspensions for flow cytometry, the left and right popliteal LNs were combined for each mouse (2 LNs/sample), minced in Click's media (Sigma-Aldrich) with 22 G needles (Exelint), and digested for 1 h at 37 °C in 94 μg/mL DNase I (Roche) and 250 μg/mL collagenase type I and 250 μg/mL collagenase type IV

(Worthington Biochemicals). Cell suspensions were passed through a 100 µm cell strainer (BD Falcon), and total viable cell numbers were enumerated by trypan blue exclusion. All single-cell suspensions were incubated for 15 minutes at 25 °C in LIVE/DEAD Fixable Viability Stain 510 (BD biosciences) to identify viable cells and then stained for 30-45 minutes at 4 °C with anti−mouse FcγRIII/ II (2.4G2; BD Pharmingen) and the following antibodies from BioLegend diluted in FACS buffer (PBS with 2% FBS): anti-CD45 (30-F11), anti-CD31 (clone 390), and anti-PDPN (8.1.1), CD54 (clone YN1/1.7.4). To evaluate OT1 division cells were stained with CD45.1 (clone A-20), CD4 (clone RM4-5), B220 (clone RA3-6B2), CD44 (clone IM7), CD8 (clone 53-6.7). Cells were washed 3 times in PBS/2% FBS and then fixed for 15 minutes in 1× PBS/1% PFA and analyzed on a Beckman Coulter CytoFlex LX flow cytometer using CytExpert software. Analysis was performed using FlowJo software version 10 (Tree Star Inc.) and GraphPad Prism version 10.1.1. Data were evaluated for statistically significant differences using a 1-way ANOVA test followed by Tukey's multiple-comparison test. $P < 0.05$ was considered statistically significant.

Immunofluorescence imaging with inhibitors
Human lymphatic endothelial cells (Promocell) were grown in complete Endothelial Cell Growth Medium MV2 (Promocell) until ~50% confluent on a thin layer of matrigel. Cells were then plated onto an 8 well chamber slide. Cells were grown until approximately 50% confluent and then treated with Clorpromazine (Sigma, 10 µg/ml) or Nystatin (Sigma, 25 µg/ml) for 1 hr before addition of 5 µg/ml OVA-488. 2 hours later cells were washed with PBS and fixed with 4% formaldehyde and then imaged on a Nikon Xi microscope. Images were taken using a 20x objective and integrated fluorescence intensity per cell was measured using ImageJ.

Human LN explant processing and staining
Human Pancreatic Lymph Nodes were removed from deceased donors (Supplementary Data S4) by the University of Colorado Pathology Shared Resource (NIH P30CA046934) and distributed to our laboratory where visible fat was removed. The lymph nodes were divided into two groups, day 1 and day 3, and cut into thirds. Tissue was placed in 1 mL of complete Endothelial Cell Growth Medium MV2 (Promocell) supplemented with antimycotic-antibiotic and treated with either 5 µg/mL of OVA-488 and 2.5 µg/mL Poly I:C, 5 µg/mL OVA-488 alone, or PBS. 14 to 19 hours after treatment the OVA 488 and Poly I:C were washed off and all media was replaced with fresh Endothelial Cell Growth Medium MV2 plus antimycotic-antibiotic. LN pieces were digested and prepared for flow cytometry on day 1 and day 3. For digestion, the tissue removed and placed into 1 mL of Click's Medium (EHAA) supplemented with 50 µL of 50 mg/mL Collagenase I, 50 µL of 50 mg/mL Collagenase IV, and 50 µL of 2.5 mg/mL Deoxyribonuclease I from Bovine Pancreas and then disrupted using scalpels followed by mincing with 22 G needles. The tissue was then placed at 37 °C. After the first 30 min, and then every 15 min for up to one-hour, the tissue was pipetted up and down 5–6 times using a 5 mL serological pipette. After digestion, the sample was passed through a 100 µm cell strainer (BD Falcon) into 3 mL of Clicks Medium (EHAA) with 5 mM EDTA and 5% FBS. The filter was washed with 5 mL of the supplemented Clicks Medium. The single cell suspension in PBS was stained with fixable viability stain 510 and washed in FACS buffer (HBSS pH7.4, 0.1% BSA, 0.02% Sodium Azide, 2 mM EDTA) before staining with CD45 (clone HI30), CD31 (clone WM59), HLA-DR (clone L243), CD14 (clone HCD14), and ICAM1 (clone HCD54) (biolegend) in human Fc block (Miltenyi). Thirty minutes later cells were washed in FACS buffer and run on a Beckman Coulter CytoFlex LX and analyzed with FlowJo software as described above.

Phosphorothioate oligonucleotides and conjugation to protein
Oligonucleotides were synthesized by Integrated DNA Technologies (IDT) with phosphorothioated oligonucleotides at every linkage as previously described in ref. 11. Oligonucleotides were conjugated to ovalbumin as previously described in ref. 11 using iEDDA-click chemistry[63]. GeoMX tags: DNA tags were provided by IDT using standard desalting and 5' Amino Modifier C6 with 70 phosphorothioate bonds. GeoMX Barcode 1 target sequence: 5'/5AmMC6/ GTTAGG AGGGTCCTTCTAATGTTAACGCCCGAATATTAGTCATATTTTGCTAGC GCCTATCAGCGTAAGA-3'; GeoMX Barcode 2 target sequence: 5'/ 5AmMC6/ GGCGATCCAGCCGGTATACCTTAGTCACATATACTATCGT AATATTGGCGGTTGCTGACAAGTAAATACG-3'. psDNA tags for single cell sequencing: psDNA2 5'/5AmMC6/ AGACGTGTGCTCTTC CGATCTNNNCCTGAATTCGAGNNNGCTCACCTATTAGCGGCTAAGG/ 3Bio/ and psDNA4 5'/5AmMC6/ AGACGTGTGCTCTTCCGATCTNNNNT-CAGGTACCTGANNNGCTCACCTATTAGCGGCTAAGG/3Bio/ (Data S5). Endotoxin levels were quantified using the Pierce Limulus Amebocyte Lysate Chromogenic Endotoxin Quantitiation kit (ThermoScientific) to be less than 0.5EU/mg for either ovalbumin or ovalbumin conjugated to psDNA. Protein concentration was measured using the Pierce BCA Protein Assay kit (ThermoScientific) and confirmed on a protein SDS gel with silver stain.

Preparation of single-cell suspensions
21 or 42 days following vaccination with 1E4 PFU of VV-WR and 20 µg of OVA-psDNA per footpad, popliteal lymph nodes were harvested from 13 mice and lymph nodes mechanically separated with 22-gauge needles in 2 mL of EHAA media. Mouse popliteal lymph nodes were split into two digestion media's. Eight popliteal LNs were digested in collagenase D (1 mg/mL) and DNase 1 (0.25 mg/mL) for 30 min at 37 °C as described previously[9] for isolation of the dendritic cells. The other 18 popliteal LNs were digested with 0.25 mg of Liberase DL (Roche, Indianapolis, IN) or Collagenase I and Collagenase IV as described above, per mL of EHAA media with DNAse 1(Worthington, Lakewood, NJ) at 37 °C to isolate the stromal cell population for 1 hr at 37 °C with pipetting every 15 min to physically agitate the digested tissues. The stromal cell digestion media was replaced with fresh digestion media after 30 min. Following digestion, cells were filtered through a screen and washed with 5 mM EDTA in EHAA + 2.5% FBS (R&D Systems: S12450). The 8 popliteal LNs digested for dendritic cells isolation were then stained with CD11c (N418), CD11b (clone #M1/70) and B220 (clone #RA3-6B2), and a live/dead dye (564406, BD Biosciences). Live cells were then sorted into four tubes on a FACS Aria Cell Sorter (BD): sorted CD11c-APC Cy7 (clone N418 1:400)+ cells, sorted CD11b PE-Cy7+ (clone M1/70,biolegend) cells, sorted B220 PE+ (clone RA3-6B2) cells and Fixable Viability Stain 510 (564406, BD Biosciences) ungated live cells, which were recombined at a 4:4:1:1 ratio, respectively. For the remaining lymph nodes in the stromal cell digest, cells were stained with CD45-PE (clone # 30-F11) and Ter119-PE (clone # TER-119) followed by magnetic bead isolation using the Miltenyi bead isolation kit. CD45-negative cells that passed through the column were then washed. Both sorted and selected (CD45+ and CD45-) cells were then washed with PBS in 0.1% BSA as described in the Cell Prep Guide (10x Genomics) and counted using a hemocytometer. Final concentration of cells was approximately 1600 cells/µL and approximately 10−20 µL were assayed.

Single-cell library preparation using the 10x Genomics platform
Cells were assayed using the 10x Genomics single-cell 3' expression kit v3 or v3 HT kit according to the manufacturer's instructions (CG000053_CellPrepGuide_RevD) and CITE-seq protocol (cite-seq.com/protocol Cite-seq_109213) with the changes outlined in ref. 11 which include cDNA amplification and cleanup and amplification of antigen tag sequencing libraries. All libraries were sequenced on an Illumina NovaSeq 6000 with 2 × 150 base pair read lengths.

Preparation of spatial transcriptomics slides
The popliteal lymph nodes were harvested either 3 or 6 weeks after immunization with 20 µg of one or both OVA-psDNA GeoMx tags and

1e4 pfu per foot of vaccinia virus. Lymph nodes were fixed for 24 h in 10% phosphate buffered formalin, and then placed in 70% Ethanol until embedding. The lymph nodes were embedded in paraffin wax, and (7 μM) sections were cut.

For analysis with the Nanostring GeoMx platform, 7 μM sections were cut from paraffin-embedded LNs as described above. Slides were stained with Lyve-1-647 (clone: EPR21771), CD11c-Biotin (clone: D1V9Y), CD4 (clone: 4SM95). The nuclei were counterstained with SYTO™ 82 Orange Fluorescent Nucleic Acid Stain (S11363). Biotinylated anti-bodies were visualized with Streptavadin-AF594 (S32356) and the CD4 antibody was visualized with OPAL 520 (FP1487001KT, Akoya Biosciences). The ROI's selected to undergo GeoMx DSP spatial transcriptomics were chosen based on Lyve-1 staining, CD11c staining and CD4 staining. Regions were selected based on the size of the area or the maximum size allowed for the ROI.

For analysis with the 10x Genomics Xenium platform, 5 μM sections were cut from paraffin-embedded lymph nodes described above using a microtome. 2 LNs were analyzed for each immunization group (21 day tag, 42 day tag, 21 and 42 day tag). We obtained Xenium data for a total of 6 individual LNs, which included 2 lymph nodes for each immunization group. For each LN we assayed two adjacent tissue sections for a total of 4 sections per immunization group. LN sections from one of the dual immunization samples came from the outer edge of the LN and were excluded from downstream analysis. Sections were placed on 10x Genomics Xenium slides, baked for 2 h at 60 C, followed by depar-affinization and decrosslinking. Oligonucleotide probe panels were used that included the 379 gene Xenium Mouse Tissue Atlassing Panel (1000627, 10x Genomics) and a custom panel (1000561, 10x Genomics) that included our antigen DNA barcode sequences and additional genes identified from our scRNA-seq data. Probes were hybridized to mRNA and spatial barcode targets in-situ and rolling circle amplification (RCA) was used to boost fluorescent signal according to the manufacturer's instructions. Tissue was imaged using the Xenium Analyzer (PN-1000569). Regions were manually defined, one region per lymph node, before capture. Each lymph node was captured in technical duplicate (two 5 uM sections per lymph node on separate Xenium slides). DAPI nuclear staining was used to identify individual cells in the automated Xenium Analyzer cell segmentation pipeline. Additional cell segmentation reagents (e.g. membrane dyes) were not applied.

scRNA-seq gene expression processing

FASTQ files for the day 2 and day 14 time points were processed as previously described in ref. 11. FASTQ files for the day 21, day 42, and dual immunized samples were processed using the Cell Ranger count pipeline (v6.0.1) and aligned to the mm10 genome. Initial filtering of gene expression data was performed in R 4.3.1 using the Seurat package (v4.4.0). The CD45+ and CD45- samples were processed separately and were combined into separate Seurat objects that included all immunization conditions (2 d, 14 d, 21 d, 42 d, dual immunized). Cells were filtered based on the number of genes expressed (>250 and <5000) and the percentage of mitochondrial reads (<20%). Genes were filtered to only include those detected in >5 cells. Gene expression reads were normalized by the total mouse reads for the cell, multiplied by a scale factor of 10,000, and log-transformed (NormalizeData). Normalized mouse counts were scaled and centered (ScaleData) using the top 2000 variable features (FindVaria-bleFeatures). The scaled data were used for PCA (RunPCA) and the samples were integrated using the Harmony package[64]. The integrated data were then used to identify clusters (FindNeighbors, FindClusters) and run UMAP (RunUMAP).

For the CD45- samples, we used the integrated cell clusters to generate an initial set of broad cell type annotations using the R package clustifyr (v1.12.0)[21] and reference data from Immgen[23]. These annotations were checked for accuracy and further refined using known cell type markers including Ptprc, Pdpn, Pecam1, Cd3e (T cells),

Cd19 and Cd79a (B cells). To annotate LEC subsets, endothelial cells were filtered, re-integrated using the Harmony package[64], and re-clustered. LEC subsets were classified using the clustifyr package along with previously published data[14].

For the CD45+ samples, we used the integrated cell clusters to generate an initial set of cell type annotations using the R package clustifyr (v1.12.0) and combined reference data from Immgen[23] along with published data for DC subsets[65]. These annotations were further refined using known cell type markers including Ptprc, Nkg7 (NK cells), Cd3e (T cells), and Cd19 (B cells). For visualization and downstream analysis, DCs were then filtered and re-integrated using the Harmony package[65].

Quantification of antigen signals

To compare antigen signals between samples, we calculated antigen scores by first dividing antigen counts present in each cell by the total number of antigen UMI counts for the library (counts per million). To account for different levels of background signal present in each library, we calculated the 75th percentile of normalized counts for B and T cells for each library. We then used this value as an estimation of background signal since B and T cells should not take up antigen. The background signal estimated for each sample was then subtracted from the normalized counts for each cell. Background corrected values that were <0 were set to 0. For visualization and downstream analysis, these background-corrected values were then log1p-transformed.

To identify antigen-high (Ag-high) and -low (Ag-low) cells, we used the calculated antigen scores for cLECs, fLECs, and collecting LECs from the day 14 time point. We used this time point since it is an intermediate time point in our time course and had distinct populations of Ag-high and Ag-low cells. We focused on cLECs, fLECs, and collecting LECs since they are the subsets with the highest overall antigen levels. For each subset we used k-means clustering to divide cells into two groups based on the day 14 antigen scores. To ensure consistent classification of Ag-high cells for each time point, we used the antigen score thresholds from the day 14 cells to identify Ag-high cells in the day 21 and day 42 time points. For the dual immunized samples, we identified Ag-high cells separately for the 21 day and 42 day antigen scores. For the day 21, day 42, and dual immunized samples, antigen signals were analyzed separately for two biological replicates. For comparison of the day 21 signal for LECs from single- and dual-immunized mice, the second biological replicate was not analyzed due to the low number of LECs captured (<40) for the single immunized sample (Figure S3D).

Prediction of antigen archiving ability and identification of archiving gene modules

To identify gene expression modules associated with antigen archiving, we used the Ag-high and Ag-low cells from day 14 cLECs, fLECs, and collecting LECs to train two distinct types of machine learning models for each LEC subset: a gradient boosting machine (GBM, model 1) and a deep neural network (DNN, model 2). Classification models were trained in R using the H2O machine learning platform (v3.44.0.3)[66]. For each LEC subset, cells were split into training (50%), validation (20%), and testing (30%) sets using stratified sampling. Due to fewer available fLECs, we used a 70/15/15 split for this subset. To identify input features for model training, we used the training and validation cells along with 10% of day 21 and day 42 cells from each LEC subset. We then identified genes that were up- or down-regulated in Ag-high cells for at least one LEC subset from at least one of the time points using the presto R package (v1.0.0). Genes were filtered to retain those expressed in >20% of cells and to remove ribosomal protein genes. Instead of using a strict p-value cutoff, we selected the top 100 genes ranked by p value and expression fold change for Ag-low and Ag-high cells from each LEC subset and each timepoint (600 genes total for each subset). Model training and hyperparameter optimization were performed using the

H2O AutoML framework using training data. Model performance was assessed using the caret R package and the top GBM and DNN models were selected based on F1 score and specificity (defined as the true negative rate), calculated using the validation data. Cells used for feature selection and model training and validation were excluded from downstream analyses. Final metrics were calculated for each model using the testing data. To identify features most predictive of antigen class for each model, variable importances were calculated internally by H2O and the top features contributing to 99% of cumulative importance were selected. Ag-high and Ag-low gene modules were then identified for each model by dividing features into two groups based on whether they were more strongly up- or down-regulated in Ag-high cells.

The top models for each LEC subset were used to predict Ag-high and -low cells in the day 14, day 21, day 42, and dual immunized samples. This was done after first excluding all cells used for feature selection and model training and validation. For time points with two biological replicates (day 21, day 42, dual immunized), we pooled both replicates together. Based on the predicted antigen classes, cells were divided into three groups, 1) has high levels of antigen based on quantified antigen scores (Ag-high), 2) has low levels of antigen but is predicted to be Ag-high (Ag-competent), or 3) has low levels of antigen (Ag-low). For the dual immunized mice, cells were divided into four groups, 1) classified as Ag-high for both antigens (double-high), 2) classified as Ag-high for only one antigen (Ag-high), 3) classified as Ag-low for both antigens but predicted to be Ag-high (Ag-competent), or 4) classified as Ag-low for both antigens (Ag-low). To compare expression of the Ag-high and Ag-low gene modules derived from each model, module scores were calculated using the Seurat package (AddModuleScore). To identify cell processes that could influence antigen archiving, gene ontology terms were identified for the Ag-high and Ag-low gene modules for each LEC subset using the clusterProfiler R package (v4.8.3). Ontology terms were filtered to only include those with >10 genes, <1000 genes, and an adjusted p-value < 0.05. P-values were calculated internally using a hypergeometric test and adjusted using Benjamini-Hochberg correction. Redundant GO terms were removed based on semantic similarity using the clusterProfiler package.

Antigen archiving ability was assessed for mock- and CHIKV-infected samples (3 biological replicates each) using previously published data[16,17]. These data were processed and cell types were annotated as previously described in ref. [16]. Ag-competent cells were predicted using the GBM and DNN models trained using day 14 cLECs, fLECs, and collecting LECs as described above. Antigen archiving ability was assessed for mock- vs CHIKV-infected mice by comparing the fraction of predicted Ag-competent cells for each biological replicate.

Assessing antigen archiving in follicular lymphoma

scRNA-seq count matrices for human follicular lymphoma samples and metastasis-free lymph node samples[47] were downloaded and processed using the Seurat R package (v4.4.0) (NormalizeData, FindVariableFeatures, ScaleData, RunPCA, RunUMAP). Samples were integrated using the Harmony R package[64]. LEC subsets were annotated using the clustifyr R package[21] with published reference data for human LEC populations[48]. To identify predicted antigen archiving competent cells, we then identified human homologs for our Ag-low and Ag-high gene programs. We then predicted Ag-competent cells for human cLECs, fLECs, and collecting LECs using the GBM (model 1) and DNN (model 2) models with expression data for the homologous genes. 13% of the input genes used for model training had no unique human homolog. We then calculated the fraction of cells predicted to be Ag-competent for each LEC subset for samples with >20 cells.

Processing of Xenium data

Data for each LN tissue section was processed as a separate "field of view" (FOV) in R 4.3.1 using the Seurat package (v4.4.0). For each slide a

separate Seurat object was generated for each FOV. Antigen tag counts were added to the objects as a separate assay. Gene expression counts for each cell were normalized (SCTransform), and PCA and UMAP were performed (RunPCA, RunUMAP) followed by clustering (FindNeighbors, FindClusters). To annotate cell types, we first generated a combined cell type reference using our scRNA-seq data for CD45+ and CD45- cells from the day 42 immunized mice (Fig. 1). To do this we combined the CD45+ and CD45- datasets and reprocessed. We then transferred cell type labels to each Xenium FOV object using Seurat (FindTransferAnchors, TransferData). These initial annotations were further refined using common marker genes including Ptprc, Cd19, and Cd3d. Antigen+ cells were identified for each cell type as any cell with >0 counts for either the 21 day or 42 day antigen barcode. LEC subsets were annotated[21] R package and published ref. [14]. To quantify the distance between DCs and Ag+ LECs, sf objects were generated using the cell boundary coordinates for each cell and the distance between each DC and each Ag+ LEC was calculated using the sf R package (v1.0-16). To identify spatial relationships between antigen-positive and other cells we used the sf package, calculating the minimum distance between the boundary of antigen-positive LECs and other cells, including dendritic cells. Cell-cell interaction enrichment was calculated for Ag +/− cells for each cell type using the Giotto R package (v4.2.1)[67] in R 4.4.2.

Processing of GeoMx DSP data

Sequencing libraries generated from the Nanostring GeoMx DSP platform were sequenced on an Illumina NovaSeq6000 at a depth of 200 million reads. FASTQ files were processed using the GeoMx NGS Pipeline v2.0 software. Downstream processing and analysis was performed in R 4.3.1 following best practices described by Nanostring using the GeomxTools (v3.4.0) R package. Data were filtered to only include segments with >1000 aligned reads, >75% of reads aligned, >80% of reads stitched, >80% of reads trimmed, and >100 estimated nuclei. Probes were filtered to remove outlier probes based on the Grubb's test and aggregated for each gene. Genes were filtered to remove those detected in <1% of segments. For gene expression data, counts were normalized based on the 75th percentile of counts present in each segment. Antigen counts were normalized based on background signals estimated using counts for negative control probes. To allow the 21 day and 42 day antigen signals to be compared together on the same plot, signals were scaled separately for each antigen (relative Ag signal, Figure S8C). To do this z-scores were calculated for the 21 day antigen signal for all regions from the 21 day and dual immunized mice, and 42 day antigen signal for all regions from the 42 day and dual immunized mice.

Reporting summary

Further information on research design is available in the Nature Portfolio Reporting Summary linked to this article.

Data availability

The processed data for all figures are available in the source data file associated with this manuscript. The scRNA-seq, Xenium spatial transcriptomics, and Nanostring GeoMx DSP data have been deposited in the NCBI GEO database (GSE281268 [https://www.ncbi.nlm.nih.gov/geo/query/acc.cgi?acc=GSE281268], GSE281265, GSE281269). Previously published antigen tracking scRNA-seq data is available in the NCBI GEO database (GSE150719 [https://www.ncbi.nlm.nih.gov/geo/query/acc.cgi?acc=GSE150719]). Previously published CHIKV scRNA-seq data is available in the NCBI GEO database (GSE243638 [https://www.ncbi.nlm.nih.gov/geo/query/acc.cgi?acc=GSE243638]). Previously published human follicular lymphoma scRNA-seq data is available in the European Genome-Phenome Archive (EGAD0001008311 [https://ega-archive.org/datasets/EGAD00001008311]). All other data are available in the article and its Supplementary files or from the corresponding author upon request. Source data are provided with this paper.

Code availability

The code used for scRNA-seq and spatial transcriptomics analysis can be found at https://doi.org/10.5281/zenodo.15871881 and https://doi.org/10.5281/zenodo.15871889.

References

1. Kim, T. S., Hufford, M. M., Sun, J., Fu, Y. X. & Braciale, T. J. Antigen persistence and the control of local T cell memory by migrant respiratory dendritic cells after acute virus infection. *J. Exp. Med* **207**, 1161–1172 (2010).
2. Kim, T. S., Sun, J. & Braciale, T. J. T cell responses during influenza infection: getting and keeping control. *Trends Immunol.* **32**, 225–231 (2011).
3. Takamura, S. et al. The route of priming influences the ability of respiratory virus-specific memory CD8+ T cells to be activated by residual antigen. *J. Exp. Med* **207**, 1153–1160 (2010).
4. Zammit, D. J., Cauley, L. S., Pham, Q. M. & Lefrancois, L. Dendritic cells maximize the memory CD8 T cell response to infection. *Immunity* **22**, 561–570 (2005).
5. Zammit, D. J., Turner, D. L., Klonowski, K. D., Lefrancois, L. & Cauley, L. S. Residual antigen presentation after influenza virus infection affects CD8 T cell activation and migration. *Immunity* **24**, 439–449 (2006).
6. Jelley-Gibbs, D. M. et al. Unexpected prolonged presentation of influenza antigens promotes CD4 T cell memory generation. *J. Exp. Med* **202**, 697–706 (2005).
7. Woodland, D. L. & Kohlmeier, J. E. Migration, maintenance and recall of memory T cells in peripheral tissues. *Nat. Rev. Immunol.* **9**, 153–161 (2009).
8. Doan, T. A. et al. Immunization-induced antigen archiving enhances local memory CD8+ T cell responses following an unrelated viral infection. *NPJ Vaccines* **9**, 66 (2024).
9. Kedl, R. M. et al. Migratory dendritic cells acquire and present lymphatic endothelial cell-archived antigens during lymph node contraction. *Nat. Commun.* **8**, 2034 (2017).
10. Tamburini, B. A., Burchill, M. A. & Kedl, R. M. Antigen capture and archiving by lymphatic endothelial cells following vaccination or viral infection. *Nat. Commun.* **5**, 3989 (2014).
11. Walsh, S. M. et al. Molecular tracking devices quantify antigen distribution and archiving in the murine lymph node. *Elife* **10** (2021).
12. Rodda, L. B. et al. Single-Cell RNA Sequencing of Lymph Node Stromal Cells Reveals Niche-Associated Heterogeneity. *Immunity* **48**, 1014–1028 e1016 (2018).
13. Takeda, A., Salmi, M. & Jalkanen, S. Lymph node lymphatic endothelial cells as multifaceted gatekeepers in the immune system. *Trends Immunol.* **44**, 72–86 (2023).
14. Xiang, M. et al. A Single-Cell Transcriptional Roadmap of the Mouse and Human Lymph Node Lymphatic Vasculature. *Front Cardiovasc Med* **7**, 52 (2020).
15. Golas, G., Alonso, J. D. & Toth, Z. Characterization of de novo lytic infection of dermal lymphatic microvascular endothelial cells by Kaposi's sarcoma-associated herpesvirus. *Virology* **536**, 27–31 (2019).
16. Lucas, C. J. et al. Chikungunya virus infection disrupts lymph node lymphatic endothelial cell composition and function via MARCO. *JCI Insight* **9** (2024).
17. Carpentier, K. S. et al. MARCO(+) lymphatic endothelial cells sequester arthritogenic alphaviruses to limit viremia and viral dissemination. *EMBO J.* **40**, e108966 (2021).
18. Zhang, R. et al. Expression of the Mxra8 Receptor Promotes Alphavirus Infection and Pathogenesis in Mice and Drosophila. *Cell Rep.* **28**, 2647–2658 e2645 (2019).
19. Zhang, R. et al. Mxra8 is a receptor for multiple arthritogenic alphaviruses. *Nature* **557**, 570–574 (2018).
20. McCarthy, M. K. et al. Chikungunya virus impairs draining lymph node function by inhibiting HEV-mediated lymphocyte recruitment. *JCI Insight* **3** (2018).
21. Fu, R. et al. clustifyr: an R package for automated single-cell RNA sequencing cluster classification. *F1000Res* **9**, 223 (2020).
22. Shay, T. & Kang, J. Immunological Genome Project and systems immunology. *Trends Immunol.* **34**, 602–609 (2013).
23. Malhotra, D. et al. Transcriptional profiling of stroma from inflamed and resting lymph nodes defines immunological hallmarks. *Nat. Immunol.* **13**, 499–510 (2012).
24. Kamath, A. T., Henri, S., Battye, F., Tough, D. F. & Shortman, K. Developmental kinetics and lifespan of dendritic cells in mouse lymphoid organs. *Blood* **100**, 1734–1741 (2002).
25. Mijanovic, O. et al. Cathepsin D-Managing the Delicate Balance. *Pharmaceutics* **13** (2021).
26. Hasan, S. et al. Multi-modal proteomic characterization of lysosomal function and proteostasis in progranulin-deficient neurons. *Mol. Neurodegener.* **18**, 87 (2023).
27. Solberg, R. et al. The Mammalian Cysteine Protease Legumain in Health and Disease. *Int J Mol Sci* **23** (2022).
28. Kumamoto, K., Stewart, T. A., Johnson, A. R. & Erdos, E. G. Prolylcarboxypeptidase (angiotensinase C) in human lung and cultured cells. *J. Clin. Invest* **67**, 210–215 (1981).
29. Koike, S. & Jahn, R. SNAREs define targeting specificity of trafficking vesicles by combinatorial interaction with tethering factors. *Nat. Commun.* **10**, 1608 (2019).
30. Lin, X. et al. RILP interacts with HOPS complex via VPS41 subunit to regulate endocytic trafficking. *Sci. Rep.* **4**, 7282 (2014).
31. Schindler, C., Chen, Y., Pu, J., Guo, X. & Bonifacino, J. S. EARP is a multisubunit tethering complex involved in endocytic recycling. *Nat. Cell Biol.* **17**, 639–650 (2015).
32. He, Y. et al. Prosaposin maintains lipid homeostasis in dopamine neurons and counteracts experimental parkinsonism in rodents. *Nat. Commun.* **14**, 5804 (2023).
33. Song, Q., Meng, B., Xu, H. & Mao, Z. The emerging roles of vacuolar-type ATPase-dependent Lysosomal acidification in neurodegenerative diseases. *Transl. Neurodegener.* **9**, 17 (2020).
34. Popova, N. V., Deyev, I. E. & Petrenko, A. G. Clathrin-mediated endocytosis and adaptor proteins. *Acta Nat.* **5**, 62–73 (2013).
35. Pamarthy, S., Kulshrestha, A., Katara, G. K. & Beaman, K. D. The curious case of vacuolar ATPase: regulation of signaling pathways. *Mol. Cancer* **17**, 41 (2018).
36. Takeda, Y. et al. ROCK2 Regulates Monocyte Migration and Cell to Cell Adhesion in Vascular Endothelial Cells. *Int. J. Mol. Sci.* **20**, (2019).
37. Lee, N., Kim, D. & Kim, W. U. Role of NFAT5 in the Immune System and Pathogenesis of Autoimmune Diseases. *Front Immunol.* **10**, 270 (2019).
38. Garcia-Alonso, S. et al. Altered proTGFalpha/cleaved TGFalpha ratios offer new therapeutic strategies in renal carcinoma. *J. Exp. Clin. Cancer Res* **40**, 256 (2021).
39. Chang, W. et al. The upregulation of TGM2 is associated with poor prognosis and the shaping of the inflammatory tumor microenvironment in lung squamous cell carcinoma. *Am. J. Cancer Res* **14**, 2823–2838 (2024).
40. Han, L. et al. High Mobility Group Box-1 Promotes Inflammation-Induced Lymphangiogenesis via Toll-Like Receptor 4-Dependent Signalling Pathway. *PLoS One* **11**, e0154187 (2016).
41. Lutter, S. & Makinen, T. Regulation of lymphatic vasculature by extracellular matrix. *Adv. Anat. Embryol. Cell Biol.* **214**, 55–65 (2014).
42. Lutter, S., Xie, S., Tatin, F. & Makinen, T. Smooth muscle-endothelial cell communication activates Reelin signaling and regulates lymphatic vessel formation. *J. Cell Biol.* **197**, 837–849 (2012).

43. Mueller, S. N. et al. Regulation of homeostatic chemokine expression and cell trafficking during immune responses. *Science* **317**, 670–674 (2007).

44. Hill, M. M. et al. PTRF-Cavin, a conserved cytoplasmic protein required for caveola formation and function. *Cell* **132**, 113–124 (2008).

45. Chetrit, D., Ziv, N. & Ehrlich, M. Dab2 regulates clathrin assembly and cell spreading. *Biochem J.* **418**, 701–715 (2009).

46. Razani, B. et al. Caveolin-1 null mice are viable but show evidence of hyperproliferative and vascular abnormalities. *J. Biol. Chem.* **276**, 38121–38138 (2001).

47. Abe, Y. et al. A single-cell atlas of non-haematopoietic cells in human lymph nodes and lymphoma reveals a landscape of stromal remodelling. *Nat. Cell Biol.* **24**, 565–578 (2022).

48. Takeda, A. et al. Single-Cell Survey of Human Lymphatics Unveils Marked Endothelial Cell Heterogeneity and Mechanisms of Homing for Neutrophils. *Immunity* **51**, 561–572 e565 (2019).

49. Lucas, E. D. et al. Type 1 IFN and PD-L1 Coordinate Lymphatic Endothelial Cell Expansion and Contraction during an Inflammatory Immune Response. *J. Immunol.* **201**, 1735–1747 (2018).

50. Pelkmans, L., Kartenbeck, J. & Helenius, A. Caveolar endocytosis of simian virus 40 reveals a new two-step vesicular-transport pathway to the ER. *Nat. Cell Biol.* **3**, 473–483 (2001).

51. Netea, M. G. et al. Defining trained immunity and its role in health and disease. *Nat. Rev. Immunol.* **20**, 375–388 (2020).

52. Netea, M. G. et al. Trained immunity: A program of innate immune memory in health and disease. *Science* **352**, aaf1098 (2016).

53. Kamada, R. et al. Interferon stimulation creates chromatin marks and establishes transcriptional memory. *Proc. Natl Acad. Sci. USA* **115**, E9162–E9171 (2018).

54. Belz, G. T., Shortman, K., Bevan, M. J. & Heath, W. R. CD8alpha+ dendritic cells selectively present MHC class I-restricted non-cytolytic viral and intracellular bacterial antigens in vivo. *J. Immunol.* **175**, 196–200 (2005).

55. Cabeza-Cabrerizo, M., Cardoso, A., Minutti, C. M., Pereira da Costa, M. & Reis e Sousa, C. Dendritic Cells Revisited. *Annu Rev. Immunol.* **39**, 131–166 (2021).

56. Desch, A. N. et al. CD103+ pulmonary dendritic cells preferentially acquire and present apoptotic cell-associated antigen. *J. Exp. Med* **208**, 1789–1797 (2011).

57. Schulz, O. & Reis e Sousa, C. Cross-presentation of cell-associated antigens by CD8alpha+ dendritic cells is attributable to their ability to internalize dead cells. *Immunology* **107**, 183–189 (2002).

58. Gerner, M. Y., Torabi-Parizi, P. & Germain, R. N. Strategically localized dendritic cells promote rapid T cell responses to lymph-borne particulate antigens. *Immunity* **42**, 172–185 (2015).

59. Quintin, J. et al. Candida albicans infection affords protection against reinfection via functional reprogramming of monocytes. *Cell Host Microbe* **12**, 223–232 (2012).

60. Saeed, S. et al. Epigenetic programming of monocyte-to-macrophage differentiation and trained innate immunity. *Science* **345**, 1251086 (2014).

61. Zhao, Y., Adams, Y. F. & Croft, M. Preferential replication of vaccinia virus in the ovaries is independent of immune regulation through IL-10 and TGF-b. *eta. Viral Immunol.* **24**, 387–396 (2011).

62. Roederer, M. Interpretation of cellular proliferation data: avoid the panglossian. *Cytom. A* **79**, 95–101 (2011).

63. van Buggenum, J. A. et al. A covalent and cleavable antibody-DNA conjugation strategy for sensitive protein detection via immuno-PCR. *Sci. Rep.* **6**, 22675 (2016).

64. Korsunsky, I. et al. Fast, sensitive and accurate integration of single-cell data with Harmony. *Nat. Methods* **16**, 1289–1296 (2019).

65. Brown, C. C. et al. Transcriptional Basis of Mouse and Human Dendritic Cell Heterogeneity. *Cell* **179**, 846–863 e824 (2019).

66. Tomas Fryda [aut, c., Erin LeDell [aut], Navdeep Gill [aut], Spencer Aiello [aut], Anqi Fu [aut], Arno Candel [aut], Cliff Click [aut], Tom Kraljevic [aut], Tomas Nykodym [aut], Patrick Aboyoun [aut], Michal Kurka [aut], Michal Malohlava [aut], Sebastien Poirier [aut], Wendy Wong [aut], Ludi Rehak [ctb], Eric Eckstrand [ctb], Brandon Hill [ctb], Sebastian Vidrio [ctb], Surekha Jadhawani [ctb], Amy Wang [ctb], Raymond Peck [ctb], Jan Gorecki [ctb], Matt Dowle [ctb], Yuan Tang [ctb], Lauren DiPerna [ctb], Veronika Maurerova [ctb], Yuliia Syzon [ctb], Adam Valenta [ctb], Marek Novotny [ctb], H2O.ai [cph, fnd]. h2o: R Interface for the 'H2O' Scalable Machine Learning Platform. 2024 2024–01-11 [cited]; 3.44.0.3Available from. https://github.com/h2oai/h2o-3.

67. Dries, R. et al. Giotto: a toolbox for integrative analysis and visualization of spatial expression data. *Genome Biol.* **22**, 78 (2021).

Acknowledgements

Author contributions

R.M.S. performed bioinformatic analysis, conceptualized experiments, drafted the paper and revised the paper, T.A.D. performed experiments, analyzed data, and drafted the paper, C.J.L. performed experiments, conceptualized experiments and revised the paper, T.S.F. performed experiments and revised the paper, I.F. performed experiments and revised the paper, V.M.O. performed experiments and revised the paper, A.M.Q. performed experiments and revised the paper, B.J.D. performed experiments and revised the paper, K.Z. performed experiments and revised the paper, M.G.H. performed experiments and revised the paper, A.U. performed experiments and analyzed data, J.R.H. conceptualized experiments and revised the paper, T.E.M. conceptualized experiments and revised the paper and B.A.J. conceptualized experiments, performed experiments, analyzed data, drafted the paper, revised the paper.

Competing interests

JRH and BAJT have a patent application filed for the Methods and Compositions for Molecular Tracking Individual Cells in vivo. U.S. Patent Application No. 63/136,798, Filed January 13, 2021; International Application No. PCT/US2022/012235, Filed January 13, 2022. The remaining authors have no competing interests.

Additional information

Supplementary information The online version contains supplementary material available at https://doi.org/10.1038/s41467-025-63543-7.

Correspondence and requests for materials should be addressed to Beth A. Jirón Tamburini.

Peer review information *Nature Communications* thanks Santiago González, who co-reviewed with Tommaso Virgilio; and the other, anonymous, reviewer(s) for their contribution to the peer review of this work. A peer review file is available.

Reprints and permissions information is available at http://www.nature.com/reprints

Publisher's note Springer Nature remains neutral with regard to jurisdictional claims in published maps and institutional affiliations.